

Detection of potential large Maya settlements in the northern Petén area (State of Campeche, Mexico) using optical and radar remote sensing



Armand LaRocque^{a,*}, Brigitte Leblon^a, Jerald Ek^b

^a Remote Sensing Laboratory, Faculty of Forestry and Environmental Management (ForEM), University of New Brunswick, Fredericton, New-Brunswick E3B 5A3, Canada

^b Department of Anthropology, Western Washington University, Bellingham, WA 98225-9083, USA

ARTICLE INFO

Keywords:

Satellite images
Landsat-8
Sentinel-1A
Petén Campechano
Maya sites

ABSTRACT

This study presents preliminary results on the detection of four potential Maya settlements (designed hereafter Sites A, B, C, and D) in the northern Petén area (State of Campeche, Mexico) often referred as the Petén Campechano, using new types of freely available Landsat-8 OLI optical and Sentinel-1A C-band dual-polarized images acquired during the dry and wet seasons. The study also uses the SRTM digital elevation model. Features extracted from the images and DEM over these potential sites were compared to corresponding features from four well-documented Maya cities located in the study area (El Mirador, Calakmul, Uxul, and Yaxnohcah), indicating similar horizontal and vertical dimensions as well as vegetation patterns. The known Maya cities and potential sites are all located adjacent to expansive seasonal wetlands (*bajos*) following a common locational pattern in Maya urban centers. Further, these sites are also located at intersections of linear features that were interpreted as potential raised causeways (*sacbeob*) documented in this and other projects. This paper examines both the implications and limitations of these findings, as well as the need for ground verification of these features in future field research.

1. Introduction

The development of complex societies in the tropical environment of the Maya Lowlands represents an anomaly in comparative studies of ancient states. The interior Maya Lowlands, a region known as Interior Elevated Region (EIR, Dunning et al., 2012) or *Mesoplano Kárstico* (Gates, 1999; Folan et al., 2015, 2017), consists of an elevated karstic plateau interspersed with extensive seasonal swamps (*bajos*). This environment presents multiple challenges for human settlement, such as unpredictable seasonal rainfall and lack of perennial water sources. Nevertheless, this environment supported the development and growth of complex urban societies for nearly two thousand years. The northern Petén region of the state of Campeche (Mexico), often referred as the *Petén Campechano*, was among the most urbanized zones in the Maya Lowlands (Ruppert and Denison Jr., 1943; Folan, 1992; Folan et al., 1995a, 1995b, 2001b, 2015; Braswell et al., 2004; Šprajc, 2008; Carrasco Vargas and Colon Gonzalez, 2005; Grube, 2005; Carrasco Vargas et al., 2009; Šprajc et al., 2010). While largely depopulated since the ninth century, this region – known in ancient times as *Uxte'tuun* – witnessed the development of the sprawling city of Calakmul and several large subordinate centers. During the Late Classic period, Calakmul was the capital of the *Kaanul* (Snake) Kingdom, an expansionist

hegemonic state that extended control over vassal city-states across the Maya Lowlands (Flannery, 1972; Marcus, 1973; Grube, 2005; Martin and Grube, 2008; Ek, 2016).

The *Snake Dynasty* established a new capital at Calakmul by 635C.E. (Current Era) and embarked on an extraordinary campaign of political expansion during the “Three Kings Period” (635–735C.E.). In the immediate political orbit of Calakmul, the *Kaanul* state exerted direct rulership over subordinate kingdoms (Marcus, 1973; Grube, 2005). More distant regions were controlled by indirect forms of domination, eventually developing into a network of vassal states stretching across much of the Maya Lowlands (Flannery, 1972; Marcus, 1973; Grube, 2005; Martin, 2005; Carrasco and Colon 2005; Folan et al., 2010; Grube et al., 2012; Ek, 2016). During this grand experiment in incipient imperialism, no other polity is mentioned as frequently in the inscriptions of both neighboring and distant city-states. A combination of the decline of the *Snake Dynasty* as a major geopolitical power as well as climatic change (Gunn et al., 2002) instigated a period of political upheaval and regional conflicts, culminating in the depopulation of most cities in the interior Maya Lowlands.

Until recently, the only significant study of the area consisted of a regional reconnaissance undertaken in the 1930s (Ruppert and Denison Jr., 1943). A series of projects in the epicenter of Calakmul have greatly

* Corresponding author.

E-mail addresses: larocque@unb.ca (A. LaRocque), bleblon@unb.ca (B. Leblon), jerald.ek@wwu.edu (J. Ek).

expanded the understanding of this ancient capital, which is currently one of the largest Classic Maya cities measured both in terms of urban scale and volume of monumental architecture (Folan, 1992; Folan et al., 1995b, 2001b; Carrasco Vargas and Colon Gonzalez, 2005; Poot Franco et al., 2017). Recent research relocated many smaller centers left unstudied since the original 1930s reconnaissance (Folan et al., 2001a; Sprajc, 2008; Sprajc et al., 2010). Research in the past two decades has begun to examine the nature of subordinate centers in the regional domain of *Uxte'tuun*, including Oxpemul (Folan et al., 2010; Domínguez Carrasco et al., 2012), Uxul (Grube and Paap, 2009; Delvendahl and Grube, 2011; Grube et al., 2012; Morales López et al., 2017), and Yaxnohcah (Reese-Taylor and Anaya Hernández, 2013; Reese-Taylor et al., 2016; Brewer et al., 2017). In aggregate, these projects have helped illuminate political and social dynamics in a densely occupied region. However, the lack of developed regional and intersite surveys has precluded contextualization of these site-based projects within the broader regional landscape.

The remote nature of the *Uxte'tuun* region – located in the expansive, unpopulated, and densely forested *Calakmul Biosphere Reserve* (Folan et al., 1992) – has proven a major impediment to regional scale research. Traditional ground survey is extremely difficult and time consuming in the Maya Lowlands due to the dense tropical forest. Satellite remote sensing can help guide ground surveys, providing a cost-effective and non-destructive method of large-scale data acquisition in remote and inaccessible areas. Remote sensing data provide one of the best methods to examine the regional distribution of population centers and integrative features that link them within the broader geopolitical landscape. The first implementation of satellite images to map archaeological features in the Maya Lowlands used low resolution Landsat images to identify urban centers, *sacbeob* segments, and other archaeological features (Folan et al., 1995a; Domínguez Carrasco and Folan, 1996; Sever, 1998; Comer and Harrower, 2013; Hixson, 2013). More recently, high spatial resolution IKONOS optical images were successfully tested to map archaeological sites in neighboring Guatemala (Saturno et al., 2007; Garrison et al., 2008).

Optical satellite images are quite difficult to use in tropical areas such as the Maya Lowlands because image acquisition is restricted to cloud-free daytime conditions, which are not common in this area. Further, optical images acquired by short wavelengths have a limited ability to penetrate the vegetation canopy. Both limitations can be overcome by using images acquired by Synthetic Aperture Radar (SAR) sensors. SAR sensors are active sensors that generate their own energy at generally longer microwave wavelengths, and thus collect imagery independent of the atmospheric conditions. Furthermore, these wavelengths are more sensitive to surface morphology, surface roughness, and soil moisture, all useful physical properties for detecting archaeological features (Lasaponara and Masini, 2013). These wavelengths are long enough (on the order of cm versus μm for the optical imagery) to allow a deeper penetration inside the dense tropical forest canopy and thus offer the possibility of detecting sub-canopy features.

In previous SAR studies, Seasat L-HH band SAR images were used to discover ancient irrigation canals and cultivated wetlands in the Yucatan peninsula (Adams, 1980; Adams et al., 1981; Pope and Dahlin, 1989, 1993; Sever, 1998). Elevation maps made from SAR imagery were used to map residential settlements around El Zotz (Guatemala) with C-band SAR imagery (Garrison et al., 2011) and Chunchucmil (Mexico) with L-band SAR imagery (Hixson, 2013). Using Landsat-8 OLI optical images, Sentinel-1C-VH and C-VV SAR images, and Alos-1 PalSAR L-HH and L-HV SAR images, LaRocque et al. (2016) mapped a network of linear features that they have interpreted as being potential intersite *sacbeob* (raised paved roads or causeways), some of which have already been field-checked in the El Mirador area (Hernández et al., 2013). *Sacbeob* are well-documented in Mesoamerica (e.g., Shaw, 2012; Folan et al., 2016), particularly in the Maya Lowlands (Folan and Stuart, 1977; Benavides Castillo, 1981; Chase and Chase, 2001; Folan et al., 2001a; Stanton and Freidel, 2005), providing concrete

archaeological indices of political linkages between Maya cities.

Airborne LiDAR (Light Detection and Ranging) have been used to detect structures in several Maya sites, such as Caracol (Weishampel et al., 2011; Chase et al., 2014a, 2014b), the Mosquito region of Honduras (Carter et al., 2012), Uxbenká (Prufer et al., 2015), Yaxnohcah (Reese-Taylor et al., 2016; Brewer et al., 2017) and northern Guatemala (Canuto et al., 2018). Unfortunately, as LiDAR requires the use of aircrafts to collect data in narrow strips, image acquisition is very expensive for a large surface such as our study area. Also, LiDAR data acquisition requires higher ground point numbers than those of regular LiDAR because of the very high dense canopy cover (Prufer et al., 2015; Golden et al., 2016). As with optical images, LiDAR data can be degraded by haze and by atmospheric humidity coming from the evapotranspiration of the vegetation. In addition, detecting human features located on hilly relief often requires multiple LiDAR flight passes, with different orientations and different incident angles (Golden et al., 2016). While suitable for detailed surveys of defined areas, LiDAR data are not suitable for large-scale regional survey. Satellite images do not have this limitation and benefit from a growing amount of high quality images freely available to the public.

Our study aims to investigate the use of new types of freely available satellite images (Landsat-8 OLI optical images and Sentinel-1 dual-polarized images) to characterize several remotely-sensed characteristics of four known Maya cities (El Mirador, Calakmul, Uxul, and Yaxnohcah), and to compare them with the ones observed over four potential unknown large settlements (provisionally labelled by LaRocque and Gadoury (2017) as Sites A, B, C and D) in northern Petén region of Campeche, Mexico. While the Landsat-8 OLI optical image will be used to characterize the vegetation over each site and determine site's horizontal dimensions, the SAR images will be used to detect large structures over the well-known Maya sites and similar structures within the undocumented sites. Such detection will also be done using the SRTM digital elevation model (DEM). In addition to testing a new methodology for exploring remote and densely forested regions, the study contributes to our understanding of the distribution of ancient population centers in a poorly documented region of the Maya area.

2. Study area

2.1. Biophysical environment

The area of interest (AOI) is located within the central Maya lowlands, in the northern part of the Petén region in southern Campeche (*Peten Campechano*, see Fig. 1). The AOI covers just under 2400 km² and is mostly within the *Calakmul Biosphere Reserve* (Folan et al., 1992; Boege, 1995). The topography is part of an extensive inland karstic plateau ranging from 50 to 400 m above sea level (Fig. 1). Karst depressions, today occupied by extensive seasonal swamps, make up approximately 45% of the landscape (Dunning et al., 2002, 2012; Folan et al., 2017).

The geological structure of the AOI belongs to the Yucatan Platform (Peterson, 1983), constituted essentially of a mantle (2 to 5 km thick) of sedimentary rocks, mainly carbonate (limestone and dolostone) and evaporite (anhydrite and gypsum). All these consolidated sediments were deposited in situ, during successive periods of marine submergence during the last 65 million of years. The local limestone was very useful to the ancient Mayas, used for monuments and sculptures as well as for production of lime for agricultural and construction purposes (Straulino et al., 2013). However, these materials are porous and easily weathered.

Structurally, the karstic plateau is characterized by an anticline with a moderate slope towards the north (Gates, 1999). On the western side of this anticline, the topographic surface tilts slowly northwestwards, towards the Gulf of Mexico. This arch structure seems to be interrupted locally by a northwest-southeast fault line following the southwest side of the *El Laberinto Bajo* (Peterson, 1983; Gates, 1999; Folan et al.,

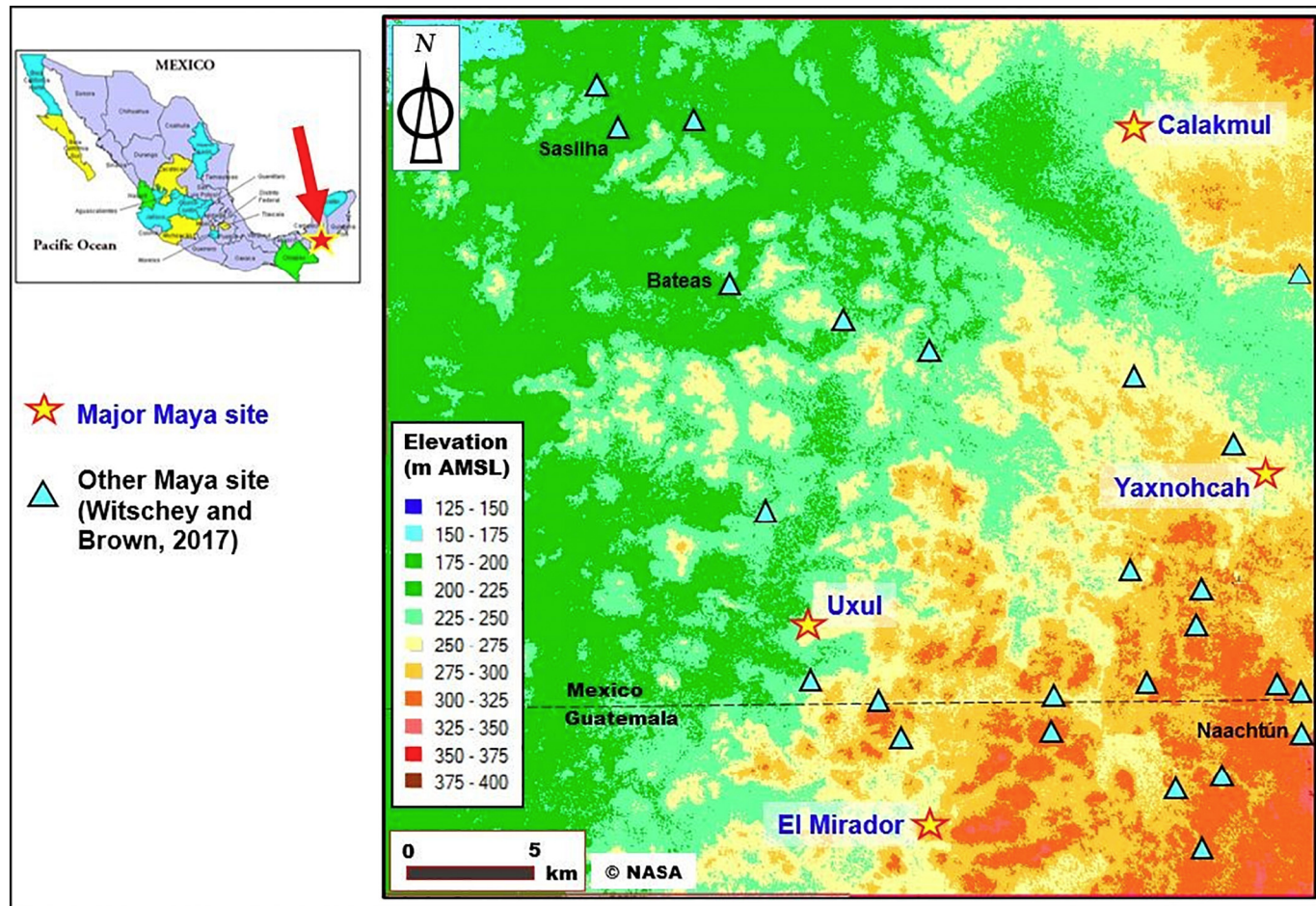


Fig. 1. Location of the study area, together with the related SRTM digital elevation model (DEM) and the location of known major and minor Maya sites (extracted from Witschey and Brown, 2017).

2017). Based on national geological investigations (INEGI, 1987a, 1987b, 1987c), no other extensive faulted structures, as the ones observed further south in central Guatemala, seem to disturb the local bedrock, except probably the presence of some local fractures without movement.

The northern Petén area is affected by a tropical climate (Gunn and Folan, 1999; INEGI, 2007; Folan et al., 2017) with strong seasonal variations in the precipitation regime (Wahl et al., 2014). The climate of the area corresponds to the “Aw” class (tropical wet savanna), a tropical climate having marked wet and dry seasons (Folan et al., 2017). Mean annual precipitation is between 1200 and 1400 mm (Giddins and Soto, 2003; INEGI, 2006). Highly seasonal rainfall patterns are defined by annual shifts in the inter-tropical convergence zone (ITCZ), with approximately 80% of annual precipitation between mid-May through November (Dunning et al., 2012). Another key element for the climate of the AOI is the difference between the annual potential evapotranspiration and annual precipitations which determines to the amount of water available for the vegetation and the humans. According to INEGI (1983) and Bauer-Gottwein et al. (2011), the potential evapotranspiration exceeds the precipitations, indicating that the study area suffers of annual water deficits. This results in the drying-out of *bajos* during the dry season (Gates, 1999) and the deposition of gypsum layers by evaporation in the bottom of *bajos* (Miller et al., 1991).

The availability of surface water in the Northern Petén is limited by the amount and distribution of rainfall, the amount of water evapotranspired by the vegetation, the mass of water present inside the soils, and the drainage of the surface runoff (Gates, 1999). Despite abundant precipitation, perennial surface water is rare due to evaporation and

seepage into the porous carbonate bedrock (Perry et al., 2003; Bautista et al., 2012; Dunning et al., 2012). Because of the lack of perennial sources of surface water, depressions transformed into storage reservoirs were critical in supporting urban populations through the dry season (Domínguez Carrasco and Folan, 1996; Weiss-Krejci and Sabbas, 2002; Perry et al., 2003; Folan et al., 2014).

Soil and vegetation types are defined by local topography, chemical composition of bedrock, and hydrology (Dunning et al., 2012, 2015). Upland soils consist mainly of Leptosols (INEGI, 2004), including Lithosols and Rendzinas classes (Morales Rosas, 1999; Bautista et al., 2012). Soils in *bajos* consist of Gleysols, Fluvisols, and Vertisols (INEGI, 2004). These shallow and poorly developed soils allow the growth of a diverse vegetation (Krasilnikov et al., 2013). The AOI is part of the tropical humid forest ecozone (Brown and Zamora Crescencio, 2017), showing a diverse range of evergreen and semi deciduous vegetation. The uplands are often covered by a dense forest (Boege, 1995; Brown and Zamora Crescencio, 2017), with mature trees reaching a height ranging from 15 to 40 m. This forest is considered as semi-evergreen, because 25 to 50% of the trees lose their leaves during the dry season (Martínez and Galindo-Real, 2002; Brown and Zamora Crescencio, 2017). In the lowlands, there are seasonal wetlands (*bajos*) which are depressions regularly flooded for two or six months and covered by herbaceous plants and sometimes by small trees with a height of less than 10 m (Martínez and Galindo-Real, 2002). All the vegetation found in *bajos* is adapted to anaerobic soil conditions, because the soil is saturated by water (Krasilnikov et al., 2013).

Table 1

Characteristics of the Sentinel-1A dual polarized images used for this study.

Conditions	Ascending orbit (*)		Descending orbit (*)	
	Date	Segment	Date	Segment
Dry	2017/01/03	14,660	2017/02/17	15,323
	2017/03/04	15,535	2017/03/01	15,498
	2017/03/16	15,710	2017/03/25	15,848
	2017/03/28	15,885	2017/04/06	16,023
	2017/04/09	16,060	2017/04/18	16,198
	2017/04/21	16,235	2017/04/30	16,373
	2017/05/27	16,760	2017/05/12	16,548
Wet	2017/06/08	16,935	2017/05/24	16,723
	2017/06/20	17,710	2017/06/05	16,898
	2017/07/12	17,285	2017/06/29	17,248
	2017/07/14	17,460	2017/07/11	17,423
	2017/07/26	17,635	2017/07/23	17,598

(*) Ascending orbit: Time UTC 00h07, Path 63, Frame 53, Polarizations VH & VV; Descending orbit: Time UTC 11h52, Path 26, Frame 530,535, Polarizations HV & HV.

2.2. Human environment

The northern Petén region was the setting for both the emergence and florescence of complex urban societies during the Formative and Classic periods. The first human occupation in the region dates to the early Middle Formative Period, with major periods of urbanization during the Late Formative and Classic Periods (Turner II et al., 2003; Folan et al., 2008). Regional reconnaissance has documented a multitude of major and minor population centers in the *Peten Campechano* (Ruppert and Denison Jr., 1943; Morales López, 1987; Šprajc, 2008; Folan et al., 2017; Morales López et al., 2017). Four large sites in the study area have been the subject of intensive archaeological survey and excavations: El Mirador, Calakmul, Uxul, and Yaxnöhcah (Fig. 1).

El Mirador, located just south of the Guatemala/Mexico border, is the largest Formative period city in the Maya lowlands (Hansen, 1990, 2001; Suyuc-Ley and Hansen, 2013; Morales Aguilar et al., 2015). Overlooking an extensive *bajo*, the urban epicenter of El Mirador consists of several major architectural complexes (Suyuc-Ley and Hansen, 2013). Located on the southwest side of the El Laberinto *bajo*, Yaxnöhcah is another major city that flourished primarily during the Formative Period (Reese-Taylor and Anaya Hernández, 2013; Haggard et al., 2017). The major Maya metropolis of Calakmul is located about 40 km north of El Mirador (Folan, 1992; Folan et al., 1995b, 2008). This sprawling city was built on the north side of the extensive El Laberinto *bajo*. One of the most important Maya cities in central lowlands, the urban center covers an area of about 2.5 km² surrounded by an urban settlement zone with 6500 structures distributed over about 30 km² (Folan, 1992; Folan et al., 2001b). Artificial reservoirs (*aguadas*) throughout the city supported the urban populace (Domínguez Carrasco and Folan, 1996). A network of linear features identified in satellite imagery, possibly *sacbeob*, radiate from the core of the city to outlying communities (Folan et al., 1995a, 2001a). Epigraphic information indicates that the *Kaanul* (Snake) Dynasty of Calakmul extended control over a much of the Maya Lowlands during the middle part of the Late Classic period (~595–695 C.E., Marcus, 1973; Grube, 2005; Martin, 2005; Martin and Grube, 2008). Located between El Mirador and Calakmul, the smaller city of Uxul is built on a small hill overlooking a large *bajo*, covering an area of 2.2 km² (Grube et al., 2012). Uxul has a shorter history strongly linked to the arrival of the powerful Snake Dynasty of Calakmul (Grube et al., 2012). The results of regional reconnaissance and site-focused projects indicate two major cycles of population expansion and urbanization during the Late Formative and Late Classic period, with depopulation of the region by the tenth century C.E (Gunn et al., 2002). For the last millennium, the area has been effectively depopulated and obscured beneath one of the largest

undisturbed tracts of continuous rainforest in Mesoamerica.

Research across the central Maya lowlands indicates population densities as high as 200 people per km² based on various archaeological indices (Turner II et al., 2003). As shown in Fig. 1, very few settlements have been documented to the west of Calakmul and El Mirador (Ford, 1995; Witschey and Brown, 2017). By contrast, Morales López (1987), Šprajc (2008), Šprajc et al. (2010), and Morales López et al. (2017) found a higher concentration of major and minor centers in the eastern part of Calakmul Biosphere Reserve. This east-west spatial difference is most likely due to the remote and inaccessible nature of the west section of the biosphere, with a high probability for undocumented cities in the latter area.

3. Materials and methods

3.1. Data

This study uses two sets of new satellite imagery that were collected mostly during the dry season (January–May), when the vegetation density is the lowest and conditions are most favorable for the detection of hidden archaeological structures (Garrison et al., 2008) and classification of local environmental diversity due to the greater contrast between wet and dry land vegetation (Pope and Dahlin, 1989). The first imagery includes twenty-four Sentinel-1C-band dual-polarized (VV and VH) SAR images which were downloaded from the European Space Agency's *Sentinels Scientific Data Hub* website (<https://scihub.copernicus.eu/>). These images were acquired between January and August 2017 (Table 1), half of them being taken during the dry season and the remaining at the beginning of the rain season. Each imagery file had two images: the VV and the VH polarized intensity images. Both images were acquired with an incidence angle between 18.3° to 46.8°. They have a 10 m spatial resolution and cover an area of 45,625 km² each. The SAR imagery was acquired during two different passes: ascending orbit with a northeast look direction, and descending orbit with a northwest look direction. According to NASA (1986), the depth of penetration of SAR microwaves into vegetation canopy depends on the radar wavelength. For C-band, this wavelength is approximatively 5.55 cm long. In a forested setting, Solberg et al. (2007) showed that C-band can penetrate through the canopy to the ground surface, before being reflected towards the SAR sensor. C band imagery over forests was also showed elsewhere to be able to map flooded grounds or soils saturated with water under a dense temperate forest (LaRocque et al., 2014).

The second imagery used is one Landsat-8 optical image that was acquired with the Operational Land Imager (OLI) sensor on March 31st, 2016. The image, which covers an area of 52,197 km², with less than 1% of cloud cover, was acquired from the USGS Global Visualization Viewer website (<http://glovis.usgs.gov/>). It contains one panchromatic band having 15 m spatial resolution and seven multispectral bands (30 m spatial resolution): B1 (coastal aerosol) (0.43–0.45 μm), B2 (blue) (0.45–0.51 μm), B3 (green) (0.53–0.59 μm), B4 (red) (0.64–0.67 μm), B5 (near-infrared or NIR) (0.85–0.88 μm), B6 (shortwave infrared 1 or SWIR-1) (1.57–1.65 μm), and B7 (shortwave infrared 2 or SWIR-2) (2.11–2.29 μm).

This study also uses a digital elevation model (DEM) to characterize the local topography and the height and width of the main features (i.e., structures, mounds, platforms or plateaus) over each site. The DEM was extracted from the *Shuttle Radar Topographic Mission* (SRTM) data available from the United States Geological Survey (<https://earthexplorer.usgs.gov/>). The SRTM DEM consists of a 1 arc-second global grid (approximately 30 m × 30 m) produced from a resampling of the original 3 arc-second grid of elevation data (approximately 90 m by 90 m) collected by the *Endeavour Space Shuttle* between 11 and 22 February 2000 (Farr et al., 2007). The DEM has a resolution of 1 m in the z-direction (elevation), recorded in m relative to Mean Sea Level (MSL).

3.2. Methodology

The Landsat-8 OLI image was processed in *PCI Geomatica 2016®*. It was first subjected to an atmospheric correction with the ATCOR program to produce a reflectance image. The 30 m multispectral band images were then pan-sharpened using the 15 m panchromatic band image with the PANSHARP program. The resulting bands have all a 15 m pixel size. The multispectral band images were then displayed in true and false color composites to determine the nature and extent of the vegetation cover and the horizontal dimensions of each site. True color composites were made with the red, green, and blue bands. False color composites were made with the near-infrared (NIR) and short-wave infrared (SWIR) bands. The NIR band (band B5 of Landsat-8) produces the maximum difference between chlorophylous vegetation and non-chlorophylous features, while the SWIR bands (bands B6 and B7 of Landsat 8) are sensitive to the difference of moisture content in the vegetation. The resulting composites images were visually photo-interpreted to determine for each site its vegetation pattern, its horizontal dimensions, and its distance to a *bajo*.

Unlike optical imagery, SAR images give complex patterns from detected objects, showing a granular aspect with a multitude of bright spots, known as speckle (Goodman, 1976). To facilitate interpretation, each Sentinel-1A image was filtered for speckle, using the “Enhanced Lee filter” of Lee et al. (2009). After filtering, each SAR image was georeferenced in the same mapping projection as the Landsat-8 OLI image (UTM 15 Q, WGS 84). Despite the speckle filtering, SAR imagery is difficult to interpret using a single image, regardless of whether the image is acquired during an ascending (Fig. 2a) or a descending orbit (Fig. 2b). Following the guidance of Dr. Thuy Le Toan to improve the image contrast, we combined the SAR images which were acquired using the same orbit. We considered first only the six images acquired during the dry season (Fig. 2c or d) and then all the twelve images acquired during both the dry and early wet seasons (Fig. 2e or f). The best contrast was achieved with all 12 SAR images (Fig. 2e and f). On the added images, we observed a signal enhancement on one side of tall objects and a shadow cast on the opposite side. These viewing effects are related to the fact that Sentinel-1A images are acquired with a side-looking radar, i.e., a radar pointing with an incident angle between 18.3° to 46.8°. Therefore, the radar beam illuminates one side of each elevated object, while the opposite side have no return signal, creating a shadowing effect (Raney, 1998). This shadow cast on SAR images enhances the visual appearance of relief and terrain structures, which is very useful for terrain analysis. The orientation of the shadow cast behind an object is directly related to the look direction of the SAR sensor. On images acquired during an ascending orbit, the shadow cast is oriented northeastwards (Fig. 2e), while it is pointing north-westwards on images collected during a descending orbit (Fig. 2f). The resulting SAR images were then displayed in *PCI Geomatica 2016®* in false color composites and then visually photo-interpreted to delineate linear or regular shape features.

A SRTM DEM was also used to produce 3D models for visualizing small spatial features using methods defined by Crysdián (2010). Topographic profiles across sites were created using methods described by Sever and Irwin (2003) to characterize the main features observed in the 3D model. These profiles were built using a 10× vertical exaggeration of 10× in order to emphasize the apparent height of the features found on the ground surface.

The methodology was first validated over the following four already documented Maya cities located in the study area: El Mirador, Calakmul, Uxul, and Yaxnöhcah. The elevation data extracted from the SRTM DEM were compared to previously published elevation maps for these sites made with ground measurements. Specific features (reservoirs, structures, and platforms) were identified on the 3D SRTM DEM model and on the SAR imagery, which is very sensitive to surface roughness. The Landsat-8 OLI image was used to identify the vegetation pattern and to determine the horizontal dimensions and distance to a

bajos. Distances from *bajos* were then compared to previously published distances for other known sites in the region. Finally, each site was located on a linear feature map produced by LaRocque et al. (2016) with Landsat-8 OLI, Sentinel-1C-band, and Alos-1 PalSAR L-band images. The methodology was then applied to four undocumented sites, called hereafter A, B, C, and D. None of the identified sites correspond to the sites already mapped by Ford (1995), Šprajc (2008), Witschey and Brown (2017) or Morales Lopez et al. (2017). One potential site (Site D) is located 1.5 km north from the documented site of Bateas, indicating that site D and Bateas could be parts of a single larger center.

4. Results

4.1. Validation over the four well-known Maya sites

4.1.1. SRTM DEM

For the site of El Mirador, the 3D model detects all three main architectural complexes of the site (Suyuc-Ley and Hansen, 2013): the pyramid of *El Tigre*, the *Grand Central Acropolis*, and the *La Danta Complex*, including the *La Pava Acropolis*, and the *Guacamaya Group* (Fig. 3a). A west-east cross section drawn over *La Danta Complex* shows the SRTM DEM elevation data are close to previously published ground measurements (Fig. 3a). For example, the *bajo* (278 m AMSL) and the platform forming the base of the complex (315 m AMSL) have the same elevation as the ones on the topographic map published by Suyuc-Ley and Hansen (2013). By contrast, the relative height (34 m) computed by subtracting the elevation of the *La Danta* pyramid base (315 m AMSL) from the elevation of its top (349 m AMSL) is smaller than the height (72 m) published by Hansen (2001), which is close to the one we measured from the surface of the *bajo* (71 m, Fig. 3a). Such a difference can be explained by the fact that the SRTM DEM has a 30 m spatial resolution, resampled from the original SRTM DEM with 90 m spatial resolution (Farr et al., 2007). A 30 m spatial resolution is not accurate enough to detect features of less than 30 m wide, such as the top of a pyramidal structure.

For Calakmul, the three largest structures mapped by Folan et al. (1995b, 2001b, 2008) are distinguishable on the SRTM DEM 3D model: West Group, Structure II, and Structure I (Fig. 3b). The *El Laberinto bajo* is also visible on the upper left corner of the SRTM DEM 3D model. On the topographic cross-section made from the DEM (Fig. 3b), the structures have well-defined profiles. The cross-section shows an artificial canal dug at the base of a hillslope, probably used to supply rainwater for large reservoirs inside the *bajo* (Folan et al., 1995b, 2001b; Domínguez and Folan 1996). The mean elevation of the *bajo* (228 m AMSL) as well as the lower (245 m AMSL) and the upper (255 m AMSL) structural terraces correspond to those observed by Folan et al. (2001b). However, the height of both Structure I (23 m) and Structure II (18 m), computed using the upper terrace as base level, is lower than the observed height (50 m and 55 m respectively) published by Folan et al. (1995b), due to the aforementioned limitation of establishing the heights from the pinnacle of pyramidal structures using the 30 m DEM.

For Uxul, the SRTM DEM 3D model shows the topographic position of the city, located on the western edge of a karstic ridge and surrounded by *bajos* on the east and south sides (Fig. 3c). The detection of large structures is less clear than for the two previous sites, likely due to the more modest size of the monumental architecture at this site. However, we are still able to locate the main architectural complexes mapped by Grube et al. (2012). Two large *aguadas* mapped by Grube et al. (2012) and Seefeld (2013) are also visible on the SRTM DEM. On a NW-SE transect over the central hill (Fig. 3c), it is possible to observe the *Aguada Occidental*, just at the foot of a steep escarpment. The difference in level between the surface of the *bajo* and the upper terrace is 47 m AMSL, giving a height of 10 m for the main structure found on the top of the hill. This height is very similar to the height (9.6 m) measured in the field for the royal palace of *Structure K2* (Grube et al., 2012).

Finally, in Yaxnöhcah, the principal central groups mapped at the

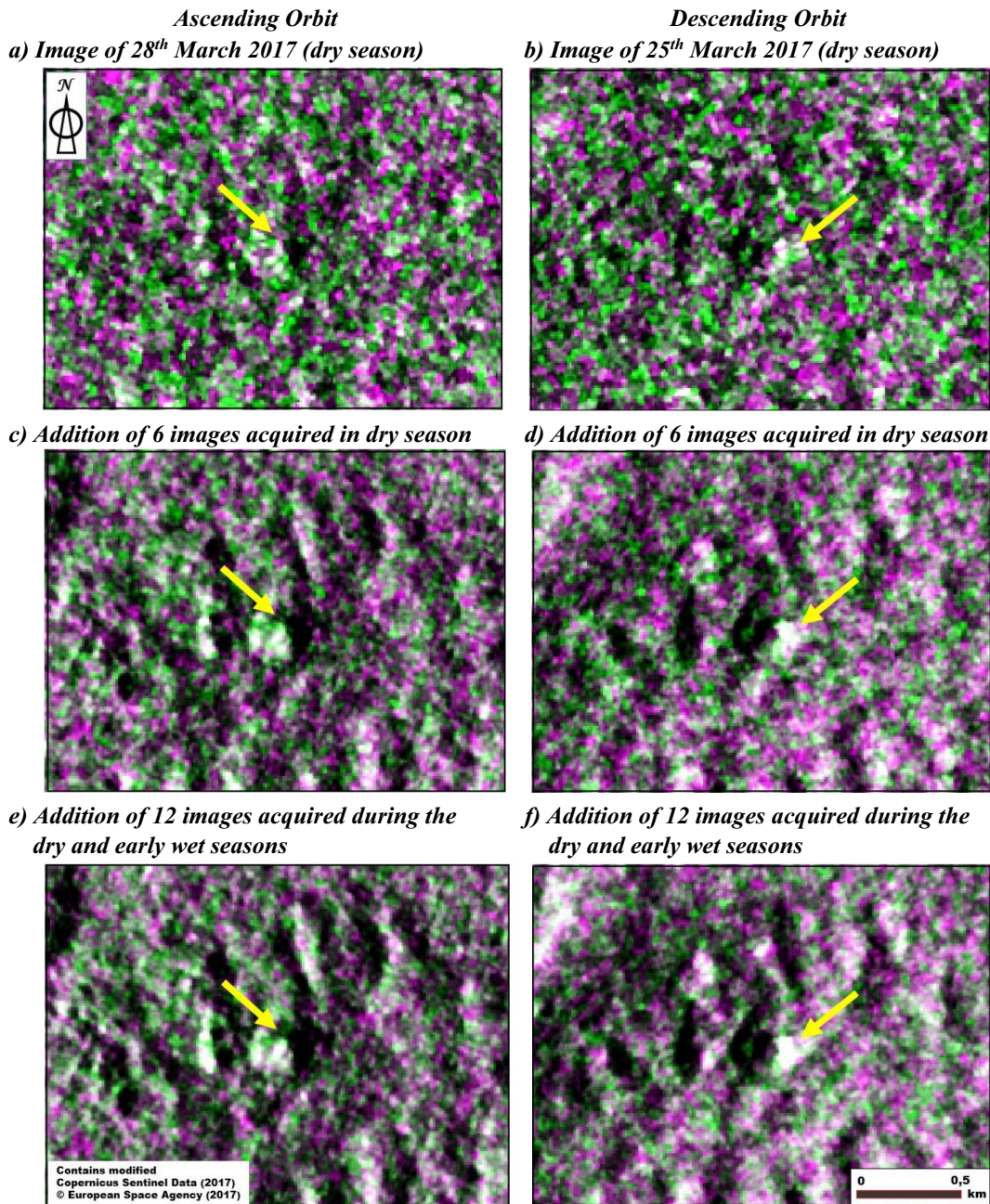


Fig. 2. Sentinel-1A C-VH and C-VV false color composite images over La Danta (arrow), just east of the city core of El Mirador (VH in red and blue, VV in green) produced with various image types acquired in 2017.

site by Šprajc (2008) and Reese-Taylor and Anaya Hernández (2013) are visible on the 3D model (Fig. 3d). From the SW-NE topographic profile derived from the SRTM DEM it is possible to detect three of the major groups of structures: Groups B, A and F. The relative height of Structure B-1 (22 m) is closed to the one published in Šprajc (2008). However, the relative height of Structure A-1 (12 m) is lower than the published ones: 24 m in Šprajc (2008) or 38 m in Reese-Taylor and Anaya Hernández (2013), because of the difficulties of acquiring accurate height measurements for the pinnacles of pyramidal structures on a 30 m DEM.

4.1.2. Sentinel-1A SAR images

The shadowing effect over the Sentinel-1A images confirms the presence of the elevated features that were detected with the SRTM DEM data (Fig. 4). For the site of El Mirador, four major features, i.e.,

the *El Tigre* pyramid, the *Grand Central Acropolis*, the *La Pava Acropolis*, and the *La Danta* pyramid, are visible on the ascending image (Fig. 4a). In addition, it is possible to discern a causeway connecting the *La Danta* Complex to the heart of the city of El Mirador (the *Calzada Danta*), which at 40 m in width is the largest documented at the city (Hernández et al., 2013). The escarpment delineating the border between the wide *bajo* and the upland is also easily visible.

The tallest structures of Calakmul are also detected on the image produced with the addition of Sentinel-1A images (Fig. 4b). Structures I and II, as well as the buildings of the West Group are also discernable due to hillshade. In addition, three of the most important municipal reservoirs mapped by Folan et al. (1995b) are visible on the image. These features appear as dark discolorations on the SAR image due to reflection from the surface of the water minimizing the signal return towards the sensor (Raney, 1998). On the upper left corner, near the

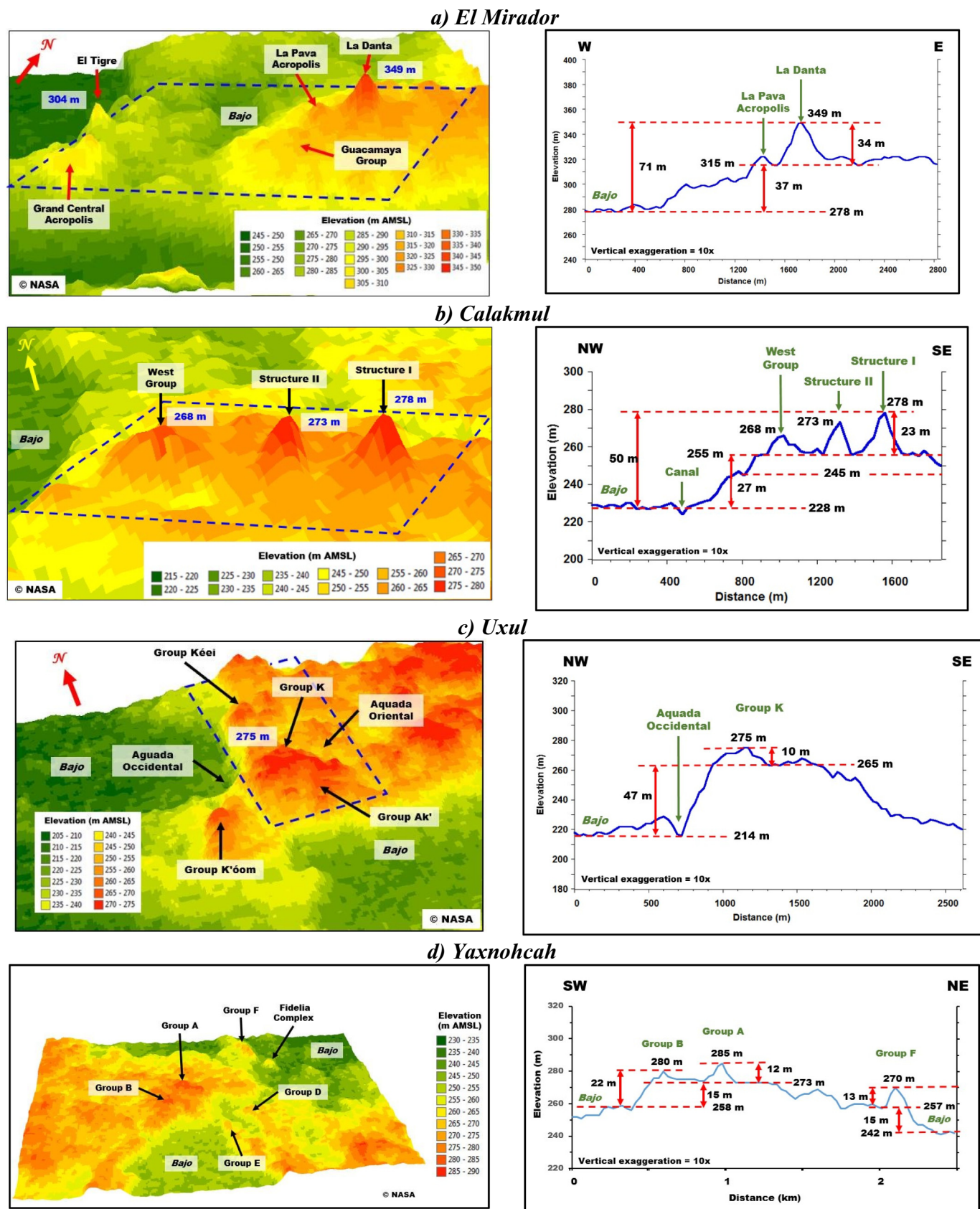


Fig. 3. 3D model extracted from the SRTM Global (1 arc sec) DEM and related topographic profile extracted from the DEM for the four well-studied Maya sites in the study area.

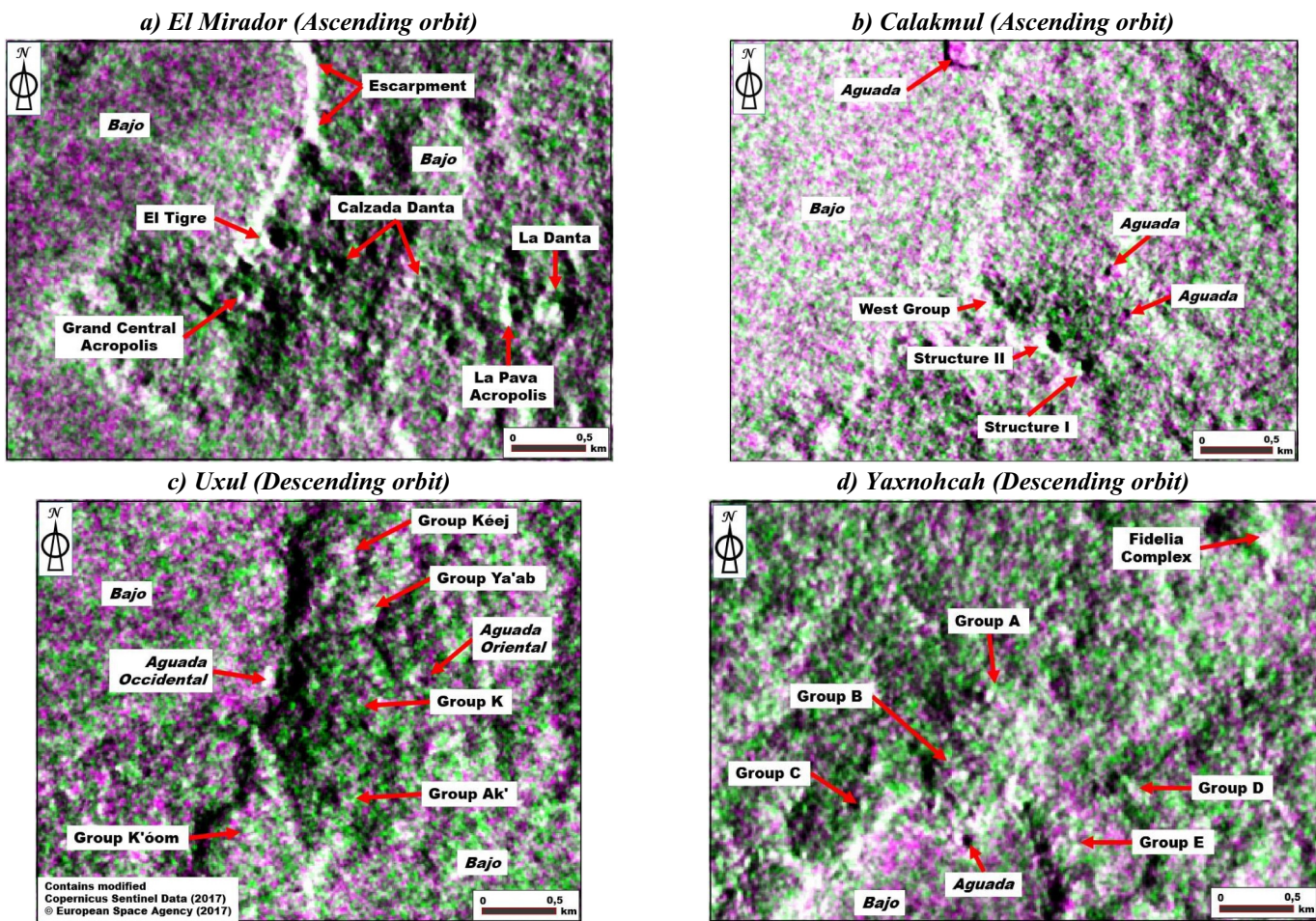


Fig. 4. Sentinel-1A C-VH and C-VV false color composite image (VH in red and blue, VV in green), produced by the addition of 12 images acquired during the dry and early wet seasons in 2017 over four well-studied Mayan sites in the study area.

margin of the *bajo*, we can see the largest documented at the site (Folan et al., 1995b, 2001b; Domínguez Carrasco and Folan, 1996).

The Sentinel-1A composite image of Uxul identifies the main groups of buildings located on a levelled hill (Fig. 4c). In contrast to the two previous sites, no notable shadow is recorded on this image due to the relatively modest height of the structures (Grube et al., 2012). However, the limit of the escarpment overlooking the border of the *bajo* is underlined by a hillshade oriented northwest. Two *aguadas* are also apparent on the SAR image and were already mapped as part of the hydraulic system of Uxul (Grube et al., 2012; Seefeld, 2013). Both have a square shape, with straight sides, making them highly visible on the SAR image.

For the site of Yaxnohcah, the Sentinel-1A images also allow identification of the main groups of buildings (Fig. 4d), including the Acropolis (Structure A-1, 24 m high) in Group A, the pyramid (Structure B-3, 23 m high) in Group B, and the platform of the *Fidelio Complex* (Reese-Taylor and Anaya Hernández, 2013). The radar image can also detect the escarpment boarding the northwest side of the *bajo* just below Group C as well as the “*Aguada Monterey*” reservoir. This reservoir is easily discernable on the SAR image due to reflection of the angled radar beam away from the sensor.

4.1.3. Landsat-8 OLI image

Both the true and false color composites made with the Landsat-8 OLI image acquired at the end of March 2016 were useful for characterization of the vegetation and buildings of the sites. For example, several white spots seen on the true color composite correspond to large structures emerging through the forest canopy, such as in El Mirador

(Fig. 5a) and Calakmul (Fig. 5b). The white color of these spots is due to the nature of the most used material by ancient Mayas to build their structures: limestone and lime sometimes mixed with earth. Some other white dots could be related with outcrops of carbonate or evaporite rocks, such as in Uxul (Fig. 5c) and Yaxnohcah (Fig. 5d). The large structures appear as a light blue to white color through vegetation on the false color composite image (Fig. 5). On both composites, *aguadas* are also easily discernable, thanks to the absence of vegetation cover and their distinctive rectangular shape, such as the ones near Calakmul (Fig. 5b), Uxul (Fig. 5c) and Yaxnohcah (Fig. 5d).

Both color composites show that the four Maya sites are located near *bajos*. These wetlands have a distinctive short vegetation, appearing different in color than the forested uplands (Fig. 5). *Bajos* have a typical blue green to cyan color on the false color composite image, due to a high reflectance in the shortwave infrared bands (B6 and B7) of Landsat-8 OLI, which are known to be sensitive to the presence of bare soil and the difference in the vegetation moisture content. The image was acquired during the dry season at the end of March 2016, when dry conditions and low vegetation coverage make the bare soil more apparent. Morales Aguilar et al. (2015) already reported that the city of El Mirador is surrounded from the south to the northwest by the *La Jarilla bajo* (Fig. 5a), a seasonal swamp covering a surface of 16 km². The proximity of *bajos* was also established for the three other Maya sites, a common location pattern across the Maya Lowlands (Adams, 1980; Folan et al., 1992; Domínguez Carrasco and Folan, 1996; Dunning et al., 2002). In each case, the distance between the center of each site and the limit of the nearest *bajo* was less than one kilometer (Table 2). These values are in agreement with those of Podobnikar and Oštir (2008),

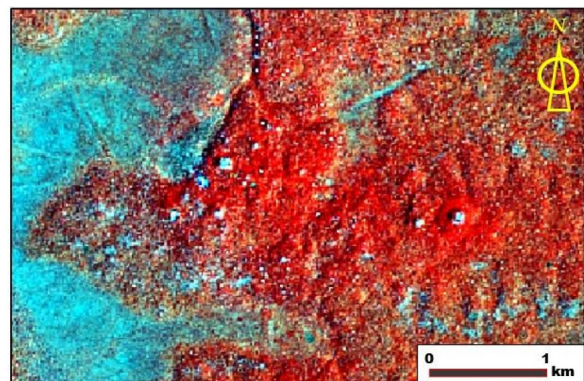
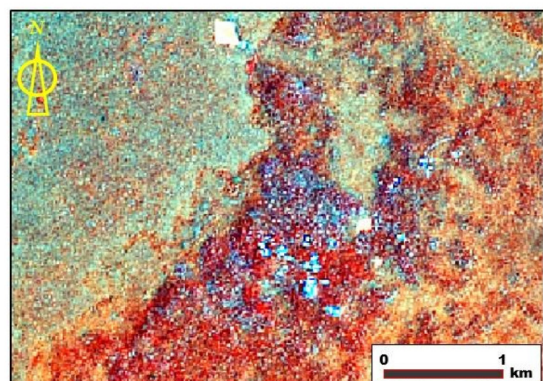
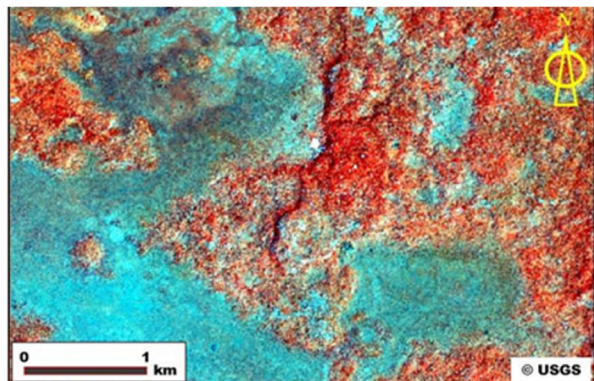
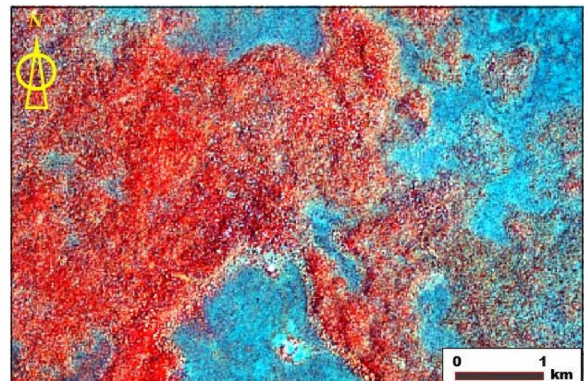
a) El Mirador*b) Calakmul**c) Uxul**d) Yaxnohcah*

Fig. 5. Vegetation pattern and site dimensions over known Mayan cities (El Mirador, Calakmul, Uxul, and Yaxnohcah) extracted from a true color composite, produced with the pan-sharpened Landsat-8 OLI image acquired on March 31st, 2016 (dry season) and corresponding false color composites (B5 in red, B6 in green, and B7 in blue).

Table 2

Comparison between known sites and potential sites in the North Petén of Campeche, Mexico.

Site	Site dimension (m)	Area (ha)	Distance between the site center and the nearest <i>bajo</i> (m)	Maximum height of the main feature (m)	Period of occupation ^(a)	Reference
El Mirador	1400 × 2800	392	500	71	1000 BCEE.–150C.E.	Suyuc-Ley and Hansen (2013)
Calakmul	1700 × 2500	425	900	50	600 BCEE.–900C.E.	Folan et al. (2008)
Uxul	1000 × 1600	160	600	57	450 BCEE.–750C.E.	Grube et al. (2012)
Yaxnohcah	1200 × 3000	360	700	38	1000 BCEE.–850C.E.	Reese-Taylor and Anaya Hernández (2013), Haggard et al. (2017)
Site A	1600 × 2500	400	900	51	NA	This study
Site B	700 × 2100	147	1300	83	NA	This study
Site C	1900 × 2900	551	1000	64	NA	This study
Site D	500 × 1000	50	1100	77	NA	This study

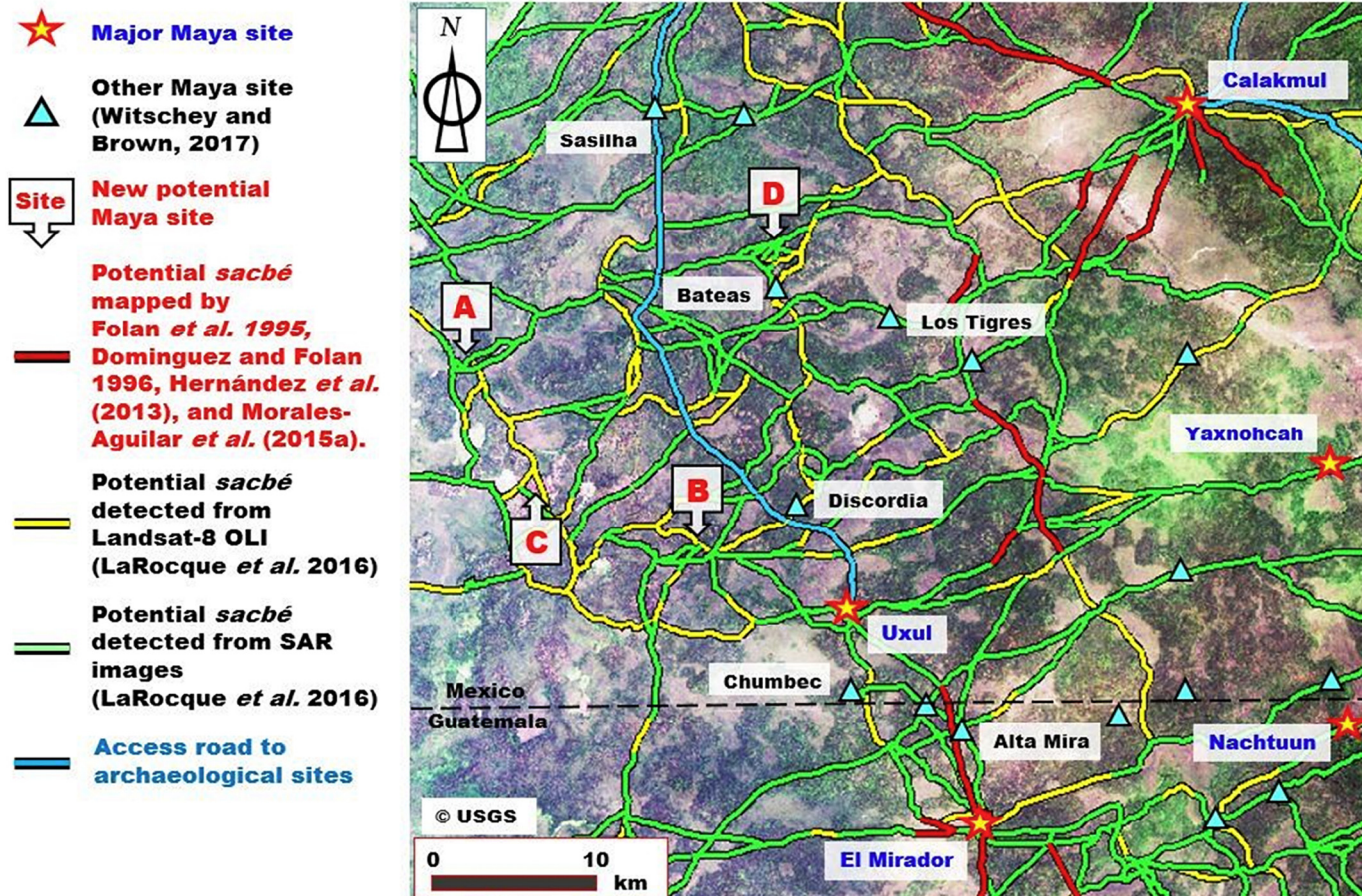
^a B.C.E. = Before Current Era; C.E. = Current Era.

Fig. 6. Network of linear features (interpreted as potential *sacbe*) mapped by LaRocque et al. (2016) from optical and radar satellite images, together with the *sacbe* segments previously mapped, the access roads, the Mayan sites as extracted from Witschey and Brown (2017)'s database, as well as the four proposed sites (A, B, C and D).

who established that the maximum distance from 63 documented sites in the region to a *bajo* is less than 2 km, with a mean distance of slightly more than 1 km. Similar patterns have been documented in the neighboring region of northern Guatemala (Sever and Irwin, 2003).

In the North Petén region, lakes and rivers are rare and ephemeral, while *bajos* cover 40% of the surface of the AOI. *Bajos* were critical for farming as they are easier to farm than the rocky hills, where Mayas built their cities (Sever and Irwin, 2003). *Bajo* margins were the best agricultural lands in the southern Maya lowlands (Dunning et al., 2015; Folan Higgins et al., 2015), where hydraulic systems can be used for flood control in the seasonal wetlands during the heavy rain season, as discovered at Calakmul (Gunn et al., 2002) and elsewhere in the Maya lowlands (Adams, 1980; Adams et al., 1981; Pope and Dahlin, 1989,

1993; Sever, 1998; Pacheco, 2016). All four sites were also located less than one kilometer from areas rich in Vertisols (INEGI, 2004). These soils would have been useful for both farming as well as a potential source of clay for ceramic production.

Both composites also reveal differences in vegetation between site centers and surrounding areas. On the true color composite, vegetation above documented sites has a lighter green color in comparison to the surrounding vegetation, indicating that deciduous trees growing over these sites keep their leaves even during dry conditions. Hardwood trees that retain leaves through the dry season have been observed in the field elsewhere in the Maya Lowlands (Nelson et al., 2017). There are multiple potential explanations for the presence of a full tree canopy over Maya sites during the dry season. First, this cannot be directly due

to soil differences, as soils in most sites consist of Leptosols, i.e., very shallow soils developed over a carbonate bedrock (INEGI, 2004). An exception is the site of Calakmul, which is associated with a dark soil rich in organic matter (Phaeozem). The most likely explanation is disturbance in the chemistry and/or hydrology of the soil due to cultural features. Indeed, Maya used limestone and lime mortar to build their stone structures, both materials being favorable to calciphilous vegetation adapted to dry conditions. The species composition of the forest located over former Maya sites could also reflect cultivation or management of economically important trees, which continue to have an impact on forest species composition into modern times (Gómez-Pompa et al., 1987; Allen et al., 2003; Dunning et al., 2015; Brown and Zamora Crescencio, 2017). One economically important tree, the *ramón* (breadnut, *Brosimum alicastrum* Swartz), is abundant on abandoned Maya structures (Lambert and Arnason, 1982; Brown and Zamora Crescencio, 2017). Other tree species, such as *sempervirens*, may have been chosen to limit evaporation during the dry season (Folan et al., 1979; Dunning et al., 2015).

The image color difference for the vegetation over both composites allows identification of the approximate boundaries of the central core of each site with a high concentration of structures (Fig. 5, Table 2). Indeed, in the central core of each site, the false color composite displays a typical red color indicating high and dense vegetation. Outside the core of sites, the upland forest is displayed with an orange color, indicating a less dense cover.

4.1.4. Linear feature map

As shown by the linear feature network previously mapped by LaRocque et al. (2016), all the four sites are located at the intersection of such features that could be interpreted as potential causeways (Fig. 6). Some segments of intersite *sacbeob* were mapped and verified in the field in previous studies (Folan et al., 1995a; Domínguez Carrasco and Folan, 1996; Hernández et al., 2013; Morales Aguilar et al., 2015). They were also easily discriminated from modern access roads and recent forest trails, which are easily visible due to the linear clearing of vegetation (LaRocque et al., 2016). This is not the case for the *sacbeob*, which are fully covered by dense vegetation. Both the raised nature and the dryness of the material make *sacbeob* detectable on SAR images that are sensitive to structural and soil moisture content changes.

4.2. Identification of potential Maya sites

4.2.1. SRTM DEM

As shown by the SRTM DEM, Site A has three major aligned mounds (A1, A2, and A3), with two other small mounds (A4, and A5) located over a raised level surface (Fig. 7a). This site is also located adjacent to *bajos*. On the topographic profile drawn from the DEM (Fig. 7a), the highest mound (A1) is 16 m tall and the remaining two others (A2 and A3) have a height of 13 m. All these mounds have a regular profile and are located over a platform having an elevation of 220 m AMSL, with a relative height difference of 32 m from the *bajos*. It is possible to detect four small holes on the surface of the *bajos* from the SRTM DEM close to the margin of the platform (Fig. 8), potentially representing reservoirs. The profile of one of these depressions is visible on the West-East cross section of the site (Fig. 7a).

For Site B, the SRTM DEM 3D model reveals the presence of a ridge delimited by two prominent mounds (B1 and B2) flanking a smaller mound (B3) (Fig. 7b). The orientation of this ridge is north-south. On the cross section across the ridge, the highest mound (B1) has a relative height of 33 m above to the surrounding terrain and 83 m above a *bajo* (210 m AMSL) located to the north (Fig. 7b). This height is much lower than the one (86 m) derived from Google Earth's image elevation data by Gadoury (2016), probably because he considered the *bajo* elevation as the base of the mound by lack of an 3D reconstruction from the landscape.

Site C is located near the *Laguna La Amapola*, a shallow intermittent

lake. It was called *K'ák'Chi* by Gadoury (2016), which means “Fire mouth” in Mayan. Six mounds are visible in the SRTM DEM situated on a hilltop almost completely surrounded by *bajos* (Fig. 7c). The SW-NE profile of the site indicated undulating terrain, with many hummocks that could represent smaller structures (Fig. 7c). Two basal platforms can be delineated at about 221 m AMSL (31 m above the elevation of the southwest *bajo*) and at 235 m AMSL, likely levelled terraces to create public plazas above the surrounding lowlands. The relative height of each mound above the second terrace is as follows: C3 (8 m), C1 (14 m), and C2 (10 m). These heights are much lower than the one (61 m) derived from Google Earth image's elevation data by Gadoury (2016), probably because he considered the *bajo* elevation as the base of each mound by lack of an 3D reconstruction of the landscape.

Site D consists of two prominent mounts located along a ridge with a SW-NE orientation surrounded by *bajos* (Fig. 7d). A transect along the long axis of the ridge reveals a large hill (277 m AMSL) supporting two prominent mounds. The largest mound (D1) has an elevation of 20 m above the surrounding hilltop platform (257 m AMSL), rising 80 m above adjacent *bajo* (197 m AMSL). Another mound (D2) on the northeast side of the hill has a height of 10 m. A lower terrace is also visible, rising 20 m above the surrounding lowlands.

This SRTM DEM data reflects notable similarities to the four well-known sites. All four potential sites are located on ecotones, particularly uplands adjacent to *bajos*, a pattern already noted by Dahlin (1983) at El Mirador and by Folan et al. (1995b, 2001b) at Calakmul. As in the documented cities, mounds within the potential sites are located on flat hills or elevated plateaus, potentially representing built platforms or modified hilltops. The topographic profile constructed from the SRTM DEM gives a good view of the surface profile for each site, facilitating distinctions between artificial structures and natural mounds. Several mounds detected on Sites A (Fig. 7a), and C (Fig. 7c) are probably man-made structures or modified natural hills as they exhibit the same regular cone shape as the major structures built in El Mirador (Fig. 3a), Calakmul (Fig. 3b), and Yaxnohcah (Fig. 3d). Their height has also the same order of magnitude (Table 2). We hypothesize that the detected mounds found over Sites A and C correspond to abandoned Maya structures, similar to the ones discovered in El Mirador, Calakmul, and Yaxnohcah, before their recent restoration. By contrast, the topographic profiles of Sites B and D is more consistent with natural hilltops given the much larger dimensions and topographic cross sections (Fig. 7b and Fig. 7d). This urban layout along a natural hilltop has been documented at the nearby site of Oxpemul (Folan et al., 2010; Domínguez Carrasco et al., 2012). Finally, the SRTM DEM data also indicate the existence of well-defined depressions near these potential Maya centers, perhaps corresponding to reservoirs. This is particularly apparent at Site A, where at least four depressions were detected in the DEM (Fig. 8). Municipal reservoirs have been documented at most known centers in the region, including Calakmul (Domínguez Carrasco and Folan, 1996), Uxul (Grube et al., 2012), and Yaxnohcah (Reese-Taylor and Anaya Hernández, 2013).

4.2.2. Sentinel-1A SAR images

As with the four known centers (Fig. 9), SAR images allow us to better visualize details in the local topography. For Site A, the Sentinel-1C-VV and C-VH false color composite image shows a distinctive rectangular shape likely corresponding to a raised platform, mostly surrounded by *bajos* (Fig. 9a). This shape was already observed on a RADARSAT-2 polarimetric SAR image by D. Delisle from the Canadian Space Agency, but it was wrongly located on Site C by Gadoury (2016). The south and east sides of the platform are highlighted by the SAR sensor during its descending orbit, producing a shadowing effect due to elevation differences between the raised platform and the surrounding wetlands located to the north and west. Due to the rectangular shape, there is a high probability that this platform is anthropogenic. Also, we cannot detect any geologic features, such as faults, fractures and other geologic lineaments on the Sentinel-1A SAR imagery around this

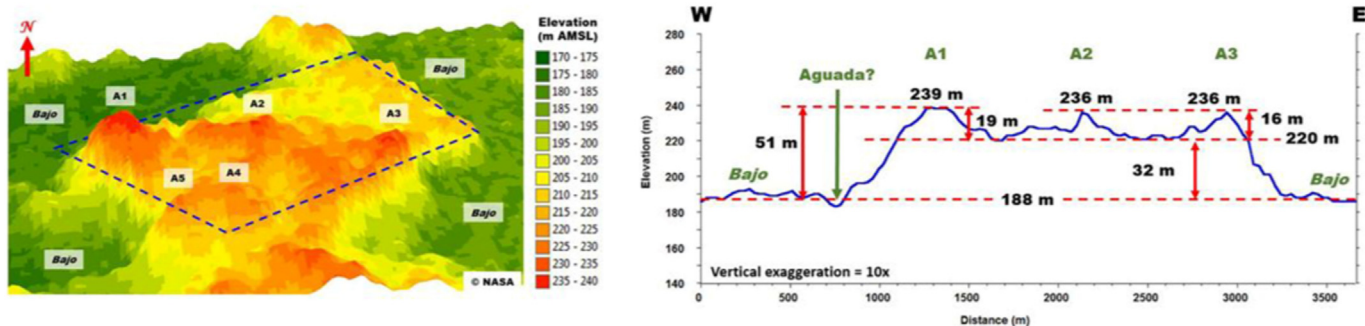
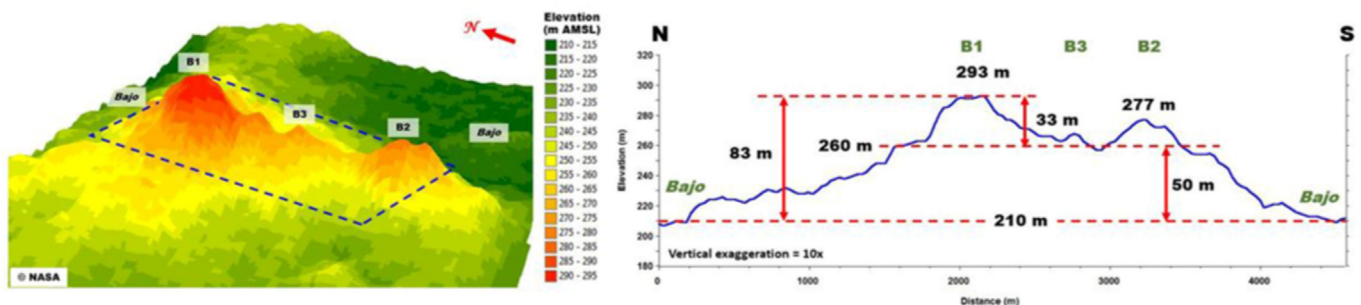
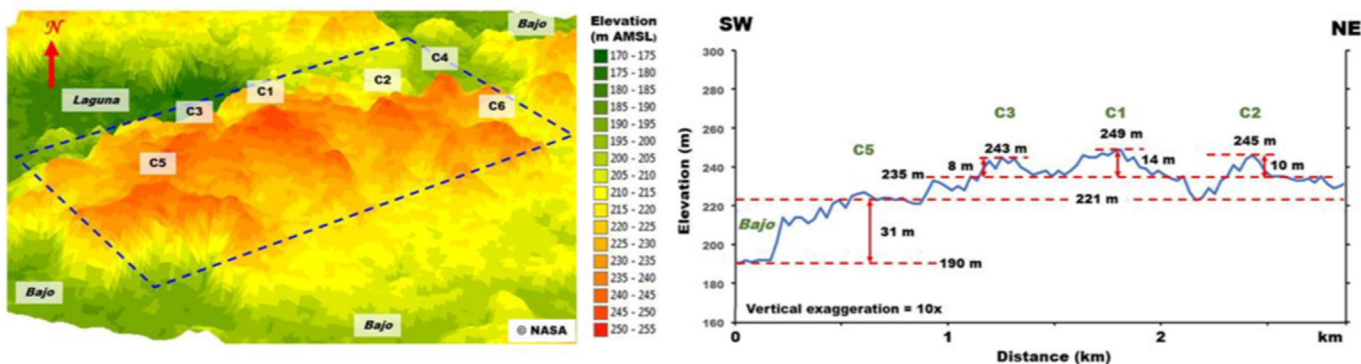
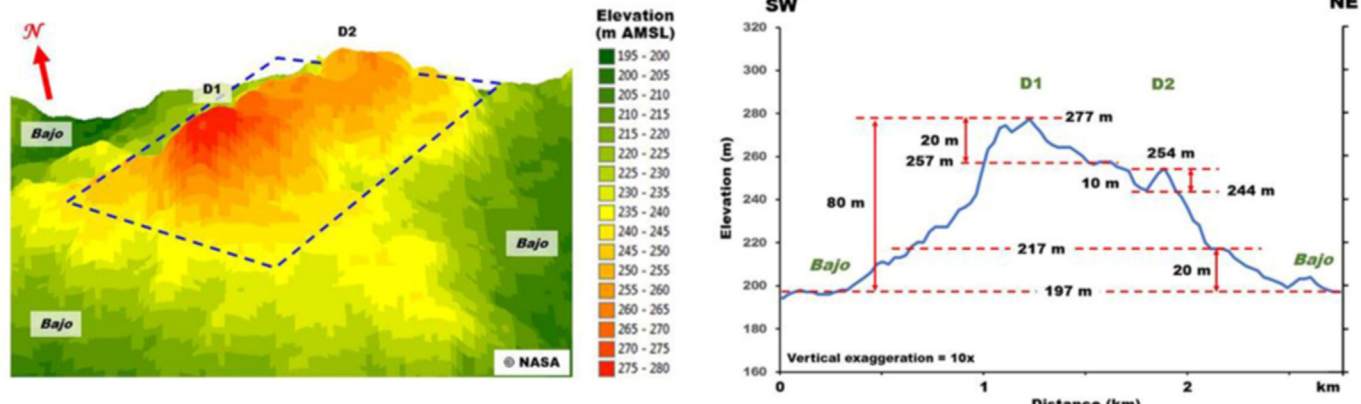
a) Site A**b) Site B****c) Site C****d) Site D**

Fig. 7. 3D model extracted from the SRTM Global (1 arc sec) DEM and related topographic profile extracted from the DEM for the four potential sites in the study area.

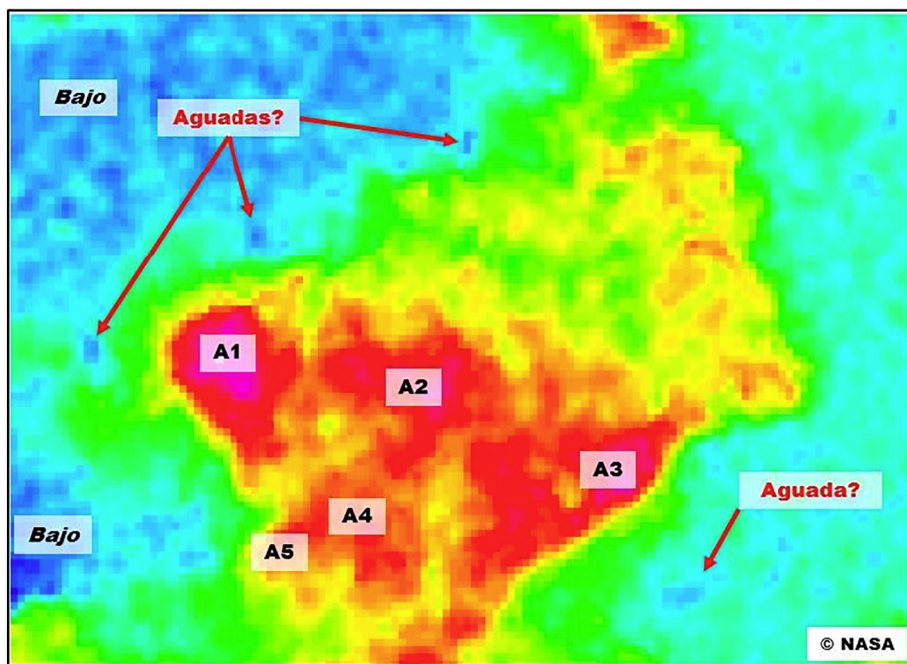


Fig. 8. Close-up of the SRTM Global (1 arc sec) DEM of site A, showing possible aquadas closed to the site (A1, A2, A3, A4, and A5 are identified mounds).

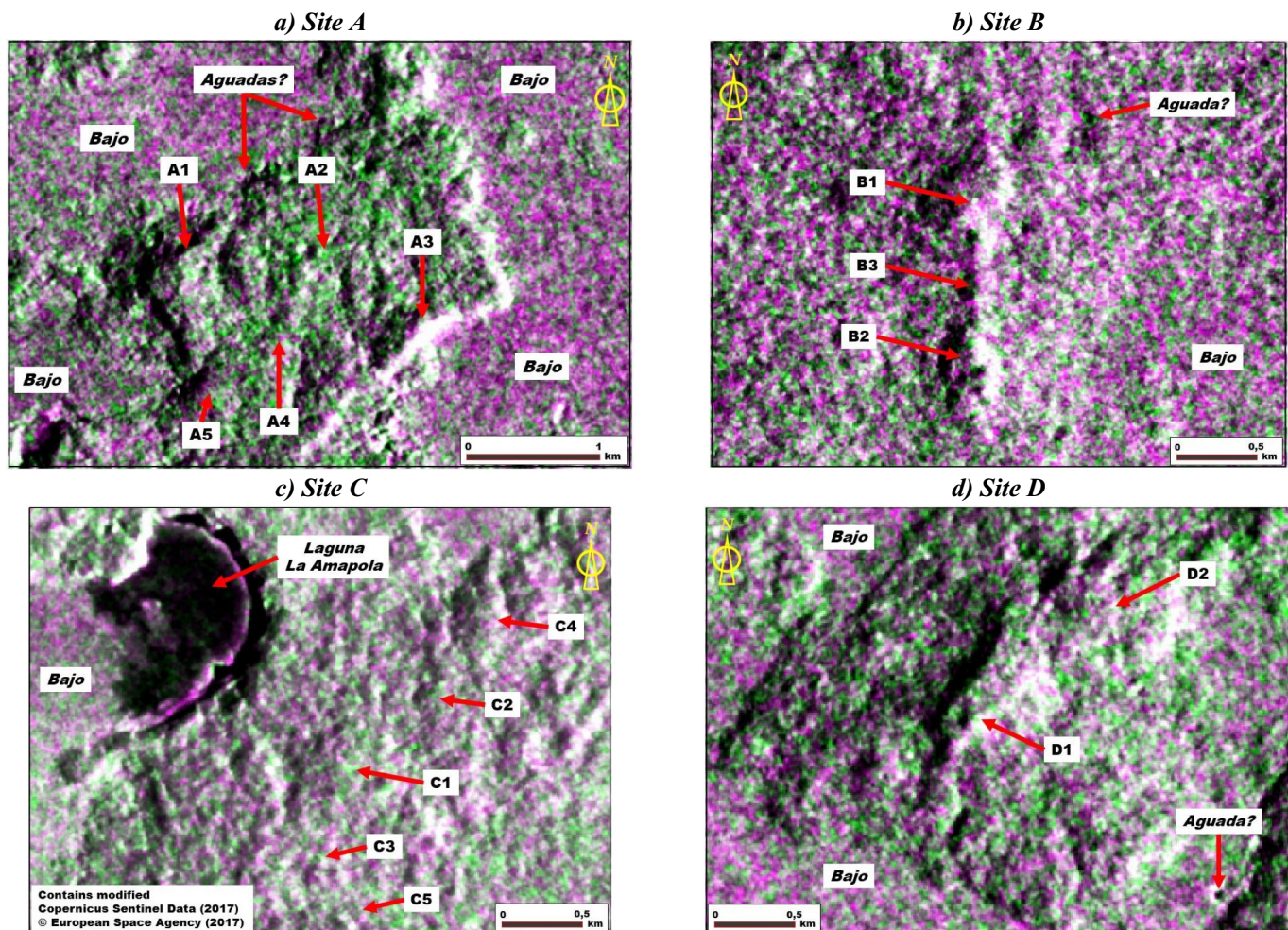


Fig. 9. Sentinel-1A C-VH and C-VV false color composite images (VH in red and blue, VV in green), produced with a addition of 12 descending orbit images acquired during the dry and early wet seasons in 2017, over the four potential sites.

feature. Further, most of the mounds detected on the SRTM DEM are also detected on the SAR image. The length of the hillshade for mounds A1, A3 and A5 indicate that they are substantial features. Finally, two of the depressions detected by the SRTM DEM in the *bajo* northwest of the platform (Fig. 8) also appears on the SAR composite image. Of the four potential undocumented sites examined in this study, Site A has the highest probability to be a former Maya settlement given its topography and spatial form, consisting of a wide, raised rectangular platform surrounding by *bajos*, with large mounds on the summit.

The three principal mounds at Site B are also visible in the radar illumination (Fig. 9b). Both mound B1 and the depression located northeast of the site were visible in the SAR hillshade and SRTM DEM. Based on its form and proximity to *bajos*, there is also a high probability that Site B represents an undocumented Maya settlement. However, as no structure-like mounds have been detected on the SRTM DEM and Sentinel-1 SAR imagery, this site is most likely a minor center.

SAR imagery from Site C (Fig. 9c) failed to detect mounds visible in the SRTM DEM, except for mounds C2 and C4. In contrast, the *Laguna La Amapola* can be distinguished by its typical dark color due to the deflection of the radar backscatter by standing water. In addition, the hillshade that follows the crescent shape of the lake contour indicates that the lake shoreline is steep, as suggested by the SRTM DEM data (Fig. 7c). Site C is a high probability location for a center due to its location on a platform close to a small intermittent lake. The regular profile of some mounds detected over this platform are similar to monumental public structures in the sample of previously documented centers, even if the vegetation cover is sparse and quite different from the other sites.

The location and substantial elevations of the two ridgeline mounds at Site D are confirmed in the SAR image (Fig. 9d). Both data sets indicate a steep slope surrounding the crest line. It is also possible to observe a rounded black spot representing a depression in the bedrock on the lower right corner of the SAR image. This water-filled depression likely represents an reservoir excavated into the hillslope. Similar to Site B, Site D is most likely a minor center.

4.2.3. Landsat-8 OLI image

As for the well-known Maya sites (Fig. 5), the true and false color composites made with the Landsat-8 OLI image acquired on March 31st, 2016, can be used to characterize the vegetation pattern over the four potential sites (Fig. 10).

On the true color composite, the vegetation covering most of sites B and D has a very bright green color (Fig. 10b and d), similar to the pattern noted at El Mirador, Calakmul, Uxul, and Yaxnohcah (Fig. 5). This light green color contrasts with the dark green color of the adjacent forested uplands and the violet color found in *bajos* (Fig. 10). The color pattern for the vegetation at sites A and C differs from the aforementioned sites. No natural factors (topographic position, bedrock composition or soils) can explain this difference for Sites A and C. Most of the vegetation covering Site A is a darker green color, except along the southeastern edge of the large platform, where there is a lighter green color, and a small rectangle occupying the mound located on the west corner with a distinctive violet color (Fig. 10a). The same violet color occurs across most of the Site C (Fig. 10c). On the false color composite, the red color is related to healthy vegetation, as is the case for most parts of sites A, B, and D (Fig. 10). There are also some areas with a cyan color corresponding to the surrounding upland forest.

Both the violet color on the true composite and the cyan color on the false composite are similar to the color displayed by the surrounding *bajos*. This is particularly the case of vegetation for the west corner of Site A (Fig. 10a), most of Site C (Fig. 10c) and parts of Site D (Fig. 10d), where the cyan color is dominant. These colors are related to a sparse tree density or loss of leaves during the dry season. The lower density of the vegetation cover could be the result from a natural recent disturbance (wildfire) or anthropogenic activity (illegal timber harvesting). Further investigation is needed to determine the reason for

this vegetation difference.

As with the documented cities, we can delineate the approximate extension of the monumental epicenters of the four potential sites sing the distinctive vegetation color detected on the Landsat-8 OLI true-color composite image (Fig. 10). The values of the measured dimensions computed for the potential sites are comparable to those of El Mirador, Calakmul, Uxul, and Yaxnohcah, with Site C having an even larger spatial extent. The small area on the southwest side of Site A has a size of 400 m by 800 m, covering a surface of 50 ha (Fig. 10a).

Bajos at all sites considered in the study have a typical violet or cyan color on the true or false color composite (Fig. 10). However, sections of some *bajos* show a greener color on the false color composite, indicating increased moisture or denser vegetation. This is particularly apparent in the south of Site D (Fig. 10d) and around Site A (Fig. 10a). The distance between the core of each site and the border of the closest adjacent *bajo* is less than 1.5 km, with a mean distance of 0.875 km (Table 2). In the case of Site C, the distance was computed from the *Laguna La Amapola*. These distances are similar to El Mirador, Calakmul, Uxul, and Yaxnohcah (Table 2).

Some small light blue to white spots may appear on the false color composite, especially within Site A (Fig. 10a), Site B (Fig. 10b), and Site D (Fig. 10d). These spots are smaller than the ones detected in the well-known Maya cities (Fig. 5). These features at the four documented cities correlate with excavations in the superstructures of the largest buildings. The existence of similar yet smaller features visible above the surrounding forest canopy in sites A, B, and D could reflect bedrock outcrops, exposed architecture, construction debris, or looter activity on the superstructures of the largest buildings.

5. Discussion and conclusions

In this study, we identified several consistent features evident in satellite imagery from previously identified sites in the central Maya lowlands to develop a formal and locational model for the identification of undocumented archaeological sites. This study identified a clear pattern in location, topography and vegetation visible in new satellite imagery (Landsat-8 OLI optical, and Sentinel-1C-VH and C-VV SAR images) and SRTM DEM data from El Mirador, Calakmul, Uxul and Yaxnohcah. The same features were identified in four potential undocumented sites using the same remote sensing data. The four potential sites were selected because they were first located at the intersections of linear features interpreted as potential causeways (*sacbeob*) by LaRocque et al. (2016). All the potential sites were located on natural platforms overlooking *bajos*, often with mounds conforming to a similar topographic profile to monumental structures in the four known cities. The Landsat-8 OLI composite image shows similar vegetation patterns between the four known sites and the potential undocumented ones. Moreover, all sites are located in similar topographic and ecological settings: near the margins of large *bajos* and associated with depressions that are likely managed reservoirs. For the four known sites, the SRTM DEM elevation data were validated with published elevation data of these sites. However, the SRTM DEM was unable to sense accurately the height of pyramidal structures or of small low structures. Indeed, the large pixel size of the SRTM DEM data (90 m resampled to 30 m) is insufficient to detect the pointed top of pyramidal structures.

The results of this study highlight multiple areas for future research. First, this research underscores the need for future reconnaissance and survey in the Calakmul region, particularly in the poorly documented western zone of Calakmul Biosphere Reserve. Despite clear evidence for the centrality of this region in prehispanic Maya historical dynamics, southeastern Campeche remains one of the more poorly understood parts of the Maya Lowlands. There is a particularly high probability for discovery of previously undocumented centers, including major cities, in the Uxte'tuun region. Further, this study tested dual polarized SAR imagery. Further work is needed to evaluate the utility of fully or compact polarimetric images, which could be used to develop improved

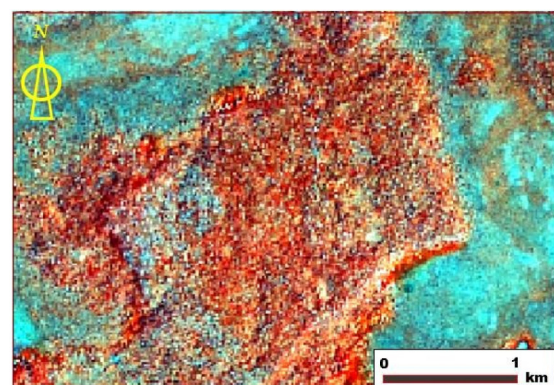
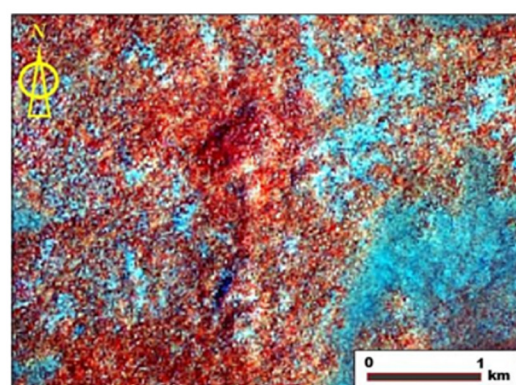
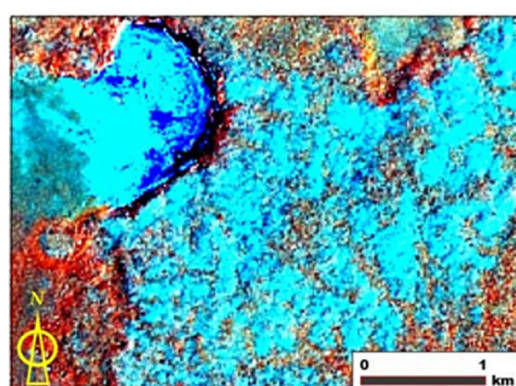
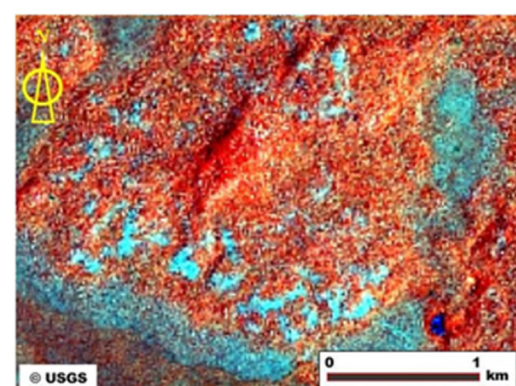
a) Site A**b) Site B****c) Site C****d) Site D**

Fig. 10. Vegetation pattern and site dimensions over the four potential Mayan sites, extracted from a true color composite, produced with the pan-sharpened Landsat-8 OLI image acquired on March 31st, 2016 (dry season) and corresponding false color composites (B5 in red, B6 in green, and B7 in blue).

tools for remotely mapping archaeological features, such as polarization synthesis, polarimetric variables, polarimetric decomposition parameters, and polarimetric signatures (Stewart et al., 2014). Further work is also needed to test higher spatial resolution DEMs produced by interferometric SAR techniques applied to free Sentinel-1, Alos PalSAR, or TanDEM-X images, which have been implemented in archaeological studies in other parts of the world (Tapete and Cigna, 2017). Additionally, the new Global DEM (NASADEM) produced by NASA that will become available in the near future will present another possible source of data for the analysis and identification of ancient settlements and cultural features (Crippen et al., 2016).

While higher resolution DEMs can also be derived with airborne LiDAR, the spatial extent of these data is currently restricted to survey zones surrounding previously documented sites. A less expensive alternative will be to use some LiDAR data acquired with the *ICESat GLAS* satellite covering some parts of the study area (Golden et al., 2016; Nelson et al., 2017). Although this satellite has been decommissioned in 2010 and the *GLAS* data only cover narrow sections of the study area with disconnected strips with a coarse spatial resolution, we are currently working to incorporate these data into a future study. While expensive, it would be advantageous to collect LiDAR data over the four potential sites in order to better characterize the nature of these potential centers and associated features such as roads, municipal water systems, and agricultural landscape modifications. Most importantly, ground verification of sites and associated cultural features are critical in testing the efficacy of the locational model developed in this paper. As archaeological sites in the region are frequent prey to illicit looting, the identification and registration of sites is a crucial first step in the development of workable cultural resource management strategies. Thus, ground verification of the results from this research could have critical repercussions in the protection of Mexico's cultural patrimony. Given that the present methodology uses free satellite imagery available across the world, it can be potentially applied to other regions of archaeological importance such as the Angkor kingdom in Southeast Asia or the Nazca region in South America.

Acknowledgments

The authors would like first to sincerely thank Dr. William J. Folan (UAC) for introducing us to Maya archaeology and for his numerous suggestions and interesting exchange of views about this part of the Yucatán Peninsula as well as for his pre-submission review of this paper. They would also thank William Gadoury for sharing the information about his Canada-Wide Science Fair project. Special thanks are due to Dr. Thuy Le Toan, Centre d'Études Spatiales de la BIOSphère (CESBIO), Toulouse (France), for her helpful suggestions to improve the results of the SAR image processing. We are also very grateful to Adrien Jalran and Damien LaRocque for their help on the image processing. We would like also to thank Dr. Antonio Benavides Castillo (INAH) and the anonymous JA-R reviewers for their helpful comments on the paper. We appreciate the contribution of Dr. Walter R. T. Witschey and Dr. Clifford T. Brown for sharing their electronic Maya database. We would like also to recognize the clarification provided by Dr. Billie L. Turner II about his interesting observations related to the predicted density of Maya population during their greatest extension. We would like also to acknowledge the University of Florida, the Paseo Pantera Consortium, and the United States Agency for International Development for the use of the "Archaeological Sites Maya Forest GIS" digital database. The Landsat-8 OLI image was provided by the United States Geological Survey (USGS). The Sentinel-1A imagery was provided by the European Space Agency (ESA). The study was funded by a NSERC Discovery grant awarded to Prof. Leblon.

References

- Adams, R.E.W., 1980. Swamps, canals, and the locations of Ancient Maya cities. *Antiquity* 54212, 206–214.
- Adams, R.E.W., Brown Jr., W.E., Culbert, T.P., 1981. Radar mapping, archeology, and ancient Maya land use. *Science* 213, 1457–1463.
- Allen, E.B., Violi, H.A., Allen, M.F., Gómez-Pompa, A., 2003. Restoration of tropical seasonal forest in Quintana Roo. In: Gómez-Pompa, A., Allen, M.F., Fedick, S.L., Jiménez-Orsonio, J.J. (Eds.), *The Lowland Maya Area: Three Millennia at the Human-wildlife Interface*. The Haworth Press Inc., New York, pp. 587–598.
- Bauer-Gottwein, P., Gondwe, B.R.N., Charvet, G., Marín, L.E., Rebollo-Vieyra, M., Merediz-Alonso, G., 2011. Review: the Yucatán Peninsula karst aquifer, Mexico. *Hydrogeol. J.* 193, 507–524.
- Bautista, F., Maldonado, D., Zinck, J.A., 2012. La clasificación maya de suelos. *Ciencia y Desarrollo* 38260, 64–70.
- Benavides Castillo, A., 1981. Los caminos de Cobá y sus Implicaciones Sociales; proyecto Cobá. Mexico City, INAH, Centro Regional del Sureste (231 p.).
- Boege, E., 1995. The Calakmul Biosphere Reserve, Mexico. UNESCO South-South Cooperation Programme, Working Papers 13, Paris (39 pp.).
- Braswell, G.E., Gunn, J.D., Domínguez Carrasco, M., Folan, W.J., Fletcher, L., Morales López, A., Glascock, M.D., 2004. Defining the terminal classic at Calakmul, Campeche. In: Demarest, A.A., Rice, P.M., Rice, D.S. (Eds.), *The Terminal Classic in the Maya Lowlands: Collapse, Transition, and Transformation*. University Press of Colorado, Boulder, pp. 162–194.
- Brewer, J.L., Carr, C., Dunning, N.P., Walker, D.S., Anaya Hernández, A., Peuramaki-Brown, M., Reese-Taylor, K., 2017. Employing airborne lidar and archaeological testing to determine the role of small depressions in water management at the ancient Maya site of Yaxnochah, Campeche, Mexico. *J. Archeol. Sci. Rep.* 13, 291–302.
- Brown, C., Zamora Crescencio, P., 2017. Flora del estado regional de Calakmul. In: Folan, W.J., Rivas Romero, P., Poot Franco J. (Eds.), *La arqueología, geología, hidrología y florística del Petén Campechano*. Universidad Autónoma de Campeche, Centro de Investigaciones Históricas y Sociales, Campeche Mexico, pp. 288–302.
- Canuto, M.A., Estrada-Belli, F., Garrison, T.G., Houston, S.D., Acuña, M.J., Kováč, M., Marken, D., Nondédo, P., Auld-Thomas, L., Castanet, C., Chatelain, D., Chiriboga, C.R., Drápela, T., Lieskovský, T., Tokovinine, A., Velasquez, A., Fernández-Díaz, J.C., Shrestha, R., 2018. Ancient lowland Maya complexity as revealed by airborne laser scanning of northern Guatemala. *Science* 361 (eau0137). <https://doi.org/10.1126/science.aau0137>.
- Carrasco Vargas, R., Colón González, M., 2005. El reino de Ka'an y la antigua ciudad Maya de Calakmul. *Arqueología Mexicana* 13 (75), 40–47.
- Carrasco Vargas, R., Vázquez López, V.A., Martín, S., 2009. Daily life of the ancient Maya recorded on murals at Calakmul, Mexico. *Proc. US Nat. Acad. Sci.* 106 (46), 19245–19249.
- Carter, W.E., Shrestha, R.L., Fisher, C.T., Leisz, S.J., 2012. Geodetic imaging: a new tool for Mesoamerican archaeology. *Eos* 93 (42), 413–415.
- Chase, A.F., Chase, D.Z., 2001. Ancient Maya causeways and site organization at Caracol, Belize. *Anc. Mesoam.* 122, 273–281.
- Chase, A.F., Chase, D.Z., Awe, J.J., Weishampel, J.F., Iannone, G., Moyes, H., Yaeger, J., Brown, M.K., 2014a. The use of LiDAR in understanding the ancient Maya landscape: Caracol and western Belize. *Adv. Archeol. Pract.* 2 (3), 147–160.
- Chase, A.F., Chase, D.Z., Awe, J.J., Weishampel, J.F., Iannone, G., Moyes, H., Yaeger, J., Brown, M.K., Shrestha, R.L., Carter, W.E., Fernandez-Díaz, J.C., 2014b. Ancient Maya regional settlement and inter-site analysis; the 2013 west-central Belize LiDAR survey. *Remote Sens.* 6 (9), 8671–8695.
- Comer, D.C., Harrower, M.J. (Eds.), 2013. *Mapping Archaeological Landscapes from Space*. Springer, New York (276 pp.).
- Crippen, R., Buckley, S., Agram, P., Belz, E., Gurrola, E., Hensley, S., Kobrick, M., Lavalle, M., Martin, J., Newmann, M., Nguyen, Q., Rosen, P., Shimada, J., Simard, M., Tung, W., 2016. NASADEM global elevation model: methods and progress. *Int. Arch. Photogram.* Remote Sens. Spatial Info. Sci. XLI-B4, 125–128.
- Crysdián, C., 2010. Digital elevation model to visualize small spatial object in 3D. *Matics Matics* 4 (1), 15–20.
- Dahlin, B.H., 1983. Climate and prehistory on the Yucatán Peninsula. *Climate Change* 5 (3), 245–263.
- Delvendahl, K., Grube, N., 2011. The last hurrah! Yukn'om Yich'aak K'ahk's final game on Uxul panel 4. *Mexicon* 23 (4), 86–88.
- Domínguez Carrasco, M., Folan, W.J., 1996. Calakmul, México: Aguadas, bajos, precipitación y asentamiento en el Petén Campechano. In: Laporte, J.P., Escobedo, H. (Eds.), *IX Simposio de Investigaciones Arqueológicas en Guatemala*. Museo Nacional de Arqueología y Etnología, Guatemala City, pp. 147–173.
- Domínguez Carrasco, M.D.R., Folan, W.J., Gates, G., González Heredia, R., Gunn, J.D., Morales López, A., Robichaux, H., Volta, B., 2012. Oxpemul, su altiplanicie kárstica ondulado-Calakmul, el preclásico: 30 años en el corazón del Petén campechano. In: Arroyo, B., Paiz, L., Mejía, H. (Eds.), *XXV Simposio de Investigación Arqueológico en Guatemala*, 2011. Ministerio de Cultura y Deportes Instituto de Antropología e Historia, Guatemala, pp. 887–901.
- Dunning, N.P., Luzzadde-Beach, S., Beach, T.P., Jones, J.G., Scarborough, V., Culbert, T.P., 2002. Arising from the bajos: the evolution of a neotropical landscape and the rise of the Maya. *Ann. Assoc. Am. Geogr.* 92, 267–283.
- Dunning, N.P., Beach, T.P., Luzzadde-Beach, S., 2012. Kax and Kol: collapse and resilience in lowland Maya civilization. *Proc. US Nat. Acad. Sci.* 109 (10), 3652–3657.
- Dunning, N.P., McCane, C., Swinney, T., Purtill, M., Sparks, J., Mann, A., McCool, J.-P., Ivenco, C., 2015. Geoarchaeological investigations in Mesoamerica move into the 21st century: a review. *Geoarchaeology* 303, 167–199.
- Ek, J.D., 2016. Pottery and politics: contextualizing the classic to postclassic transition in Champotón, Campeche. *Lat. Am. Antiq.* 27 (4), 527–548.
- Farr, T.G., Rosen, P.A., Caro, E., Crippen, R., Duren, R., Hensley, S., Kobrick, M., Paller, M., Rodriguez, E., Roth, L., Seal, D., Shaffer, S., Shimada, J., Umland, J., Werner, M., Oskin, M., Burbank, D., Alsdorf, D., 2007. The shuttle radar topography mission. *Rev.*

- Geophysics 45 (RG2004), 1–33. <https://doi.org/10.1029/2005RG000183>.
- Flannery, K.V., 1972. The cultural evolution of civilizations. *Annu. Rev. Ecol. Syst.* 3, 399–426.
- Folan, W.J., 1992. Calakmul, Campeche: a centralized urban administrative center in the Northern Petén. *World Archaeol.* 24, 158–168.
- Folan Higgins, W.J., Domínguez Carrasco, M.D.R., Gunn, J.D., Morales López, A., González Heredia, R., Villanueva García, G., Torrescano Valle, N., 2015. Calakmul: power, perseverance, and persistence. In: Cucina, A. (Ed.), *Archaeology and Bioarchaeology of Population Movement among the Prehispanic Maya*. Springer, New York, pp. 37–50.
- Folan, W.J., Stuart, G., 1977. El Proyecto Cartográfico Arqueológico de Cobá, Quintana Roo. *Informes Interinos* 1, 2, 3. In: *Boletín de la Escuela Antropológica de la Universidad de Yucatán* 4 22–23, pp. 14–81.
- Folan, W.J., Fletcher, L.A., Kintz, E.R., 1979. Fruit, fiber, bark, and resin: social organization of a Maya urban center. *Science* 204 (4394), 679–701.
- Folan, W.J., García, Ortega, Sánchez, J.M., González, M.C., 1992. Programa de manejo de la Reserva de la Biosfera Calakmul PMRBC. Primer borrador. Coordinadores Juan José Consejo Dueñas, asesor, 4 volúmenes. Campeche Mexico: Universidad Autónoma de Campeche, Centro de Investigaciones Históricas y Sociales Secretaría de Desarrollo Social.
- Folan, W.J., Marcus, J., Miller, W.F., 1995a. Verification of a Maya settlement model through remote sensing. *Camb. Archaeol. J.* 5, 277–283.
- Folan, W.J., Marcus, J., Pinceman, S., Domínguez Carrasco, M., Fletcher, L.A., Morales, A., 1995b. Calakmul: new data from an ancient Maya capital in Campeche, Mexico. *Lat. Am. Antiq.* 6, 310–334.
- Folan, W.J., May Hau, J., Marcus, J., Miller, W.F., González Heredia, R., 2001a. Los caminos de Calakmul, Campeche. *Anc. Mesoam.* 12, 293–298.
- Folan, W.J., Fletcher, L.A., May Hau, J., Florey Folan, L., 2001b. Las Ruinas de Calakmul, Campeche, México: Un Lugar Central y su Paisaje Cultural. Universidad Autónoma de Campeche, Centro de Investigaciones Históricas y Sociales, Campeche.
- Folan, W.J., Fletcher, L.A., May Hau, J., Morales López, A., Domínguez Carrasco, M.D.R., González Heredia, R., Gunn, J.D., Tiesler, V., 2008. Calakmul, Campeche, México: patterns representative of its urban capital and regional state. In: Mastache, A.G., Cobean, R.H., García Cook, A., Hirth, K.G. (Eds.), *El Urbanismo en Mesoamérica, Urbanism in Mesoamerica*. Instituto Nacional de Antropología e Historia, Mexico, pp. 285–347.
- Folan, W.J., Domínguez Carrasco, M.D.R., González Heredia, R., Morales López, A., Paredes Gómez, J., Pastrana Pleitos, I., Gunn, J.D., 2010. Oxpemul, Campeche, México: de ciudad tributaria a ciudad/estado en el Petén campechano con la salida de los kanes chanes y la subida de la dinastía del trono de piedra. Los Investigadores de la Cultura Maya. 19 (2). pp. 105–131.
- Folan, W.J., González Heredia, R., Domínguez Carrasco, M.D.R., Florey Folan, L., 2014. Calakmul, Oxpemul y Coba: un patrón hidráulico en el mesoplano y plano kárstico de la Península de Yucatán, México. Los Investigadores de la Cultura Maya. 22 (2). pp. 307–324.
- Folan, W.J., Domínguez Carrasco, M.D.R., Gunn, J.D., Morales López, A., González Heredia, R., Villanueva García, G., Torrescano Valle, N., 2015. Calakmul: power, perseverance, and persistence. In: Cucina, A. (Ed.), *Archaeology and Bioarchaeology of Population Movement among the Prehispanic Maya*. Springer, London, pp. 37–50.
- Folan, W.J., Bolles, D.D., Ek, J.D., 2016. On the trail of Quetzalcoatl/Kukulcan: tracing mythic interaction routes and networks in the Maya lowlands. *Anc. Mesoam.* 27 (2), 293–318.
- Folan, W.J., Gates, G., Gunn, J.D., Volta, B., 2017. Geología, hidrología y clima. In: Folan, W.J., Poot Franco, P., Rivas Romero, J. (Eds.), *La Arqueología, Geología, Hidrología y Florística del Petén Campechano*. Universidad Autónoma de Campeche, Centro de Investigaciones Históricas y Sociales, Campeche Mexico, pp. 16–24.
- Ford, A., 1995. Archaeological Sites Maya Forest GIS. University of California, USCB Open Data, Santa Barbara. http://spatialdiscovery-ucsb.opendata.arcgis.com/datasets/1a3a1295bf2e4cafab64580182d15367_0, Accessed date: 15 October 2017.
- Gadoury, W., 2016. À la recherche depuis l'Espace de la cité maya perdue: K'ák' Chi' (Bouche du Feu). Poster presented at the Canada-Wide Science Fair, Montréal (Québec), May 2016.
- Garrison, T.G., Houston, S.D., Golden, C., Inomata, T., Nelson, Z., Munson, J., 2008. Evaluating the use of IKONOS satellite imagery in lowland Maya settlement archaeology. *J. Archaeol. Sci.* 35 (10), 2770–2777.
- Garrison, T.G., Chapman, B., Houston, S., Roman, E., Garrido López, J.L., 2011. Discovering ancient Maya settlements using airborne radar elevation data. *J. Archaeol. Sci.* 38 (7), 1655–1662.
- Gates, G., 1999. Fisiografía, geología e hidrología. In: Folan, W.J., Sánchez, M.C., Ortega, J.M. (Eds.), *Naturaleza y Cultura en Calakmul*, Campeche. Universidad Autónoma de Campeche, Centro de Investigaciones Históricas y Sociales, Campeche, pp. 31–39.
- Giddins, L., Soto, M., 2003. Rhythms of precipitation in the Yucatán Peninsula. In: Gómez-Pompa, A., Allen, M.F., Fedick, S.L., Jiménez-Orsonio, J.J. (Eds.), *The Lowland Maya Area: Three Millennia at the Human-wildlife Interface*. The Haworth Press Inc., New York, pp. 77–89.
- Golden, C., Murtha, T., Cook, B., Shaffer, D.S., Schroder, W., Hermitt, E.J., Firpi, O.A., Scherer, A.K., 2016. Reanalyzing environmental Lidar data for archaeology: Mesoamerican applications and implications. *J. Archaeol. Sci.* Rep. 9, 293–308.
- Gómez-Pompa, A., Flortes, J.S., Sosa, V., 1987. The “pet-kot”, a man-made tropical forest of the Maya. *Interciencia* 12, 10–15.
- Goodman, J.W., 1976. Some fundamental properties of speckles. *J. Opt. Soc. Am.* 66 (11), 1145–1150.
- Grube, N., 2005. Toponyms, emblem glyphs, and the political geography of southern Campeche. *Anthropol. Notebooks* 11, 89–102.
- Grube, N., Paap, I., 2009. Uxul, Petén Campechano, primera temporada de campo, 2009. In: Los Investigadores de la Cultura Maya. 18. pp. 7–24.
- Grube, N., Delvendahl, K., Seefeld, N., Volta, B., 2012. Under the rule of the snake kings, uxul in the 7th and 8th centuries. In: *Estudios de Cultura Maya*. 40. pp. 11–49.
- Gunn, J.D., Folan, W.J., 1999. Clima actual. In: Folan Higgins, W.J., Sánchez González, M.C., García Ortega, J.M. (Eds.), *Naturaleza y cultura en Calakmul, Campeche*. Universidad Autónoma de Campeche, Centro de Investigaciones Históricas y Sociales, Campeche, pp. 19–30.
- Gunn, J.D., Foss, J.E., Folan, W.J., Dominguez Carrasco, M., Faust, B.B., 2002. Bajo sedimentos and the hydraulic system of Calakmul, Campeche, Mexico. *Anc. Mesoam.* 13 (2), 297–315.
- Haggard, A., Brewer, J., Peuramaki-Brown, M., 2017. Investigations of peri-urban settlement and domestic reservoirs, research from Yaxnöhcah, Campeche. In: *Mexico. Proc. 82nd Annual Meeting of the Soc. Am. Archeol.*, Vancouver, British Columbia tDAR id: 431223.
- Hansen, R.D., 1990. Excavations in the Tigre complexes, El Mirador, Petén, Guatemala. In: *Papers of the New World Archaeological Foundation*. Brigham Young University, Provo (308 pp.).
- Hansen, R.D., 2001. The first cities, the beginnings of urbanism and state formation in the Maya Lowlands. In: Grube, N. (Ed.), *Maya, Divine Kings of the Rain Forest*. Konemann, Bonn, pp. 50–65.
- Hernández, E., Schreiner, T., Morales Aguilar, C., 2013. Uso público, uso privado y mitos asociados a las calzadas y sacbeob de El Mirador. In: Arroyo, B., Mendez Salinas, L. (Eds.), *Proc. XXVI Simposio de Investigaciones arqueológicas en Guatemala 2012. Museo Nacional de Arqueología y Etnología, Guatemala City*, pp. 939–950.
- Hixson, D.R., 2013. The use of multispectral imagery and airborne synthetic aperture radar for the detection of archaeological sites and features in the western Maya wetlands of Chunchucmil, Yucatan, Mexico. In: Comer, D.C., Harrower, M.J. (Eds.), *Mapping Archaeological Landscapes from Space*. Springer, New York, pp. 133–144.
- INEGI, 1983. Carta de evapotranspiración y déficit de agua Serie I. Escala 1:1000000. México: Instituto Nacional de Estadística Geográfica y Informática. <http://www.beta.inegi.org.mx/temas/mapas/climatologia/> [Accessed October 15, 2017].
- INEGI, 1987a. Carta geologica, Serie I, Campeche E15–6. Escala 1:250000. México: Instituto Nacional de Estadística Geográfica y Informática. <http://www.beta.inegi.org.mx/temas/mapas/geologia/> [Accessed October 13, 2017].
- INEGI, 1987b. Carta geologica, Serie I, Quintana Roo E16–4–7. Escala 1:250000. México: Instituto Nacional de Estadística Geográfica y Informática. <http://www.beta.inegi.org.mx/temas/mapas/geologia/> [Accessed October 13, 2017].
- INEGI, 1987c. Carta geologica, Serie I, Tabasco E15–9. Escala 1:250000. México: Instituto Nacional de Estadística Geográfica y Informática. <http://www.beta.inegi.org.mx/temas/mapas/geologia/> [Accessed October 13, 2017].
- INEGL, 2004. Mapa edafología. México: Instituto Nacional de Estadística Geográfica y Informática. <http://en.www.inegi.org.mx/temas/mapas/edafologia/> [Accessed October 13, 2017].
- INEGI, 2006. Carta climatológicas, Precipitación media anual. Escala 1: 1000000. México: Instituto Nacional de Estadística Geográfica y Informática. <http://www.beta.inegi.org.mx/temas/mapas/climatologia/> [Accessed October 17, 2017].
- INEGI, 2007. Carta climatológicas, Temperatura media anual. Escala 1: 1000000. México: Instituto Nacional de Estadística Geográfica y Informática. <http://www.beta.inegi.org.mx/temas/mapas/climatologia/> [Accessed October 15, 2017].
- Krasilnikov, P., Gutiérrez-Castorena, M., Del, C., Ahrens, R.J., Cruz-Gastardo, C.O., Sedov, S., Solleiro-Rebolledo, E., 2013. *The Soils of Mexico* (188 pp.). Springer, Dordrecht.
- Lambert, J.D.H., Arnason, J.T., 1982. Ramón and Maya ruins, an ecological, not an economic, relation. *Science* 216 (4343), 298–299.
- LaRocque, A., Gadoury, W., 2017. Mapping potential Maya sites in the Péten Campechano area (state of Campeche, Mexico) using optical and radar remote sensing. In: *Proceeding 37th Canadian Remote Sensing Symposium (Earth Observation Summit 2017)*, June 20–22, Montréal, QC, Canada, Abstract#478, . https://sommetot2017-eosummit2017.exordo.com/files/papers/478/initial_draft/Montreal2017-CRSS_Maya_sites.pdf, Accessed date: 19 September 2017.
- LaRocque, A., Leblon, B., Woodward, R., Mordini, M., Bourgeau-Chavez, L., Landon, A., French, N., McCarthy, J., Huntington, T., Camill, P., 2014. Use of radarsat-2 and Alos-PalSAR SAR images for wetland mapping in New Brunswick. In: *Proc. 2014 IEEE Geosci. Remote Sens. Symp.* pp. 1226–1229.
- LaRocque, A., Leblon, B., Folan, W.J., 2016. Detección de sacbeob utilizando óptica e radar imágenes. In: *Proc. XXVI Encuentro Internacional Los Investigadores de la Cultura Maya, Campeche: Universidad Autónoma de Campeche, Dirección General de Difusión Cultural*, (in press).
- Lasaponara, R., Masini, N., 2013. Satellite synthetic aperture radar in archaeology and cultural landscape, an overview. *Archeol. Prospect.* 20 (2), 71–78.
- Lee, J.S., Wen, J.-H., Ainsworth, T.L., Chen, K.S., Chen, A.J., 2009. Improved sigma filter for speckle filtering of SAR imagery. *IEEE Trans. Geosci. Remote Sens.* 47 (1), 202–213.
- Marcus, J., 1973. Territorial organization of the lowland classic Maya. *Science* 180, 911–916.
- Martin, S., 2005. Of snakes and bats, shifting identities at Calakmul. *PARI J.* 6 (2), 5–15.
- Martin, S., Grube, N., 2008. Chronicle of the Maya Kings and Queens (240 p.). Thames and Hudson, New York.
- Martínez, E., Galindo-Real, C., 2002. La vegetación de Calakmul, Campeche, México, clasificación, descripción y distribución. *Bol. Soc. Bot. Méx.* 71, 7–32.
- Miller, W.F., Siver, T.L., Lee, D., 1991. Applications of ecological concepts and remote sensing technologies in archaeological site reconnaissance. In: Sever, C.A., Behrens T.L. (Eds.), *Applications of space-age Technology in Anthropology*, Bay Saint Louis: NASA John C. Stennis Space Center, Science and Technology Lab. 109365. NASA Tech. Rep, pp. 121–136.
- Morales Aguilar, C., Mauricio, D., Hansen, R.D., Hernández, E., 2015. Los suburbios de la antigua ciudad de El Mirador, Petén, Guatemala. In: Arroyo, B., Mendez Salinas, L.,

- Paiz, L. (Eds.), Proc. XXVIII Simposio de Investigaciones arqueológicas en Guatemala, 2014. Museo Nacional de Arqueología y Etnología, Guatemala City, pp. 497–509.
- Morales López, A., 1987. Arqueología de Salvamento en la nueva carretera a Calakmul, Municipio de Champotón, Campeche. Información, 12, 75–109. Universidad Autónoma de Campeche, Centro de Investigaciones Históricas y Sociales, Campeche.
- Morales López, A., González Heredia, R., Folan, W.J., 2017. Los sitios y sus mapas. In: Folan, W.J., Poot Franco, P., Rivas Romero, J. (Eds.), La Arqueología, Geología, Hidrología y Florística del Petén Campechano. Universidad Autónoma de Campeche, Centro de Investigaciones Históricas y Sociales, Campeche, pp. 25–238.
- Morales Rosas, J., 1999. Suelos. In: Folan, W.J., Sánchez, M.C., Ortega, J.M. (Eds.), Naturaleza y Cultura en Calakmul, Campeche. Universidad Autónoma de Campeche, Centro de Investigaciones Históricas y Sociales, Campeche, pp. 41–49.
- NASA, 1986. Shuttle Imaging Radar-C Science Plan (180 pp.). NASA, Jet Propulsion Laboratory, Pasadena.
- Nelson, R., Margolis, H., Montesano, P., Sun, G., Cook, B., Corp, L., Andersen, H.E., De Jong, B., Pellar, T., Fickel, F.P., Kauffman, J., Prisley, S., 2017. Lidar-based estimates of aboveground biomass in the continental US and Mexico using ground, airborne, and satellite observations. *Remote Sens. Environ.* 188, 127–140.
- Pacheco, E.V., 2016. La alimentación en Itzamkanac El Tigre, agricultura, caza, pesca y comercio. In: Proc. XXVI Encuentro Internacional Los Investigadores de la Cultura Maya. Universidad Autónoma de Campeche, Dirección General de Difusión Cultural, Campeche (*in press*).
- Perry, E., Velasquez-Oliman, G., Socki, R.A., 2003. Hydrogeology of the Yucatán Peninsula. In: Gómez-Pompa, A., Allen, M.F., Fedick, S.L., Jiménez-Orsonio, J.J. (Eds.), The Lowland Maya Area, Three Millennia at the Human-wildlife Interface. The Haworth Press Inc., New York, pp. 115–138.
- Peterson, J.A., 1983. Petroleum geology and resources of southeastern Mexico, northern Guatemala, and Belize. USGS Circ. 760 (44 pp.).
- Podobnikar, O., Oščir, K., 2008. Geographic information system and remote sensing analysis. In: Šprajc, I. (Ed.), Reconocimiento arqueológico en el Sureste del Estado de Campeche, México, 1996–2005. British Archeol. Rep., Oxford, pp. 243–261.
- Poot Franco, P., Rivas Romero, J., Folan, W.J., Morales López, A., González Heredia, R., 2017. Análisis e interpretación de datos. In: Folan, W.J., Rivas Romero, P. Poot Franco J. (Eds.), La Arqueología, Geología, Hidrología y Florística del Petén Campechano. Universidad Autónoma de Campeche, Centro de Investigaciones Históricas y Sociales, Campeche, pp. 303–333.
- Pope, K.O., Dahlin, B.H., 1989. Ancient Maya wetland agriculture, new insights from ecological and remote sensing research. *J. Field Archeol.* 16 (1), 87–106.
- Pope, K.O., Dahlin, B.H., 1993. Radar detection and ecology of Ancient Maya canal systems - reply to Adams et al. *J. Field Archeol.* 20 (3), 379–383.
- Prufer, K.M., Thompson, A.E., Hennett, D.J., 2015. Evaluating airborne LiDAR for detecting settlements and modified landscapes in disturbed tropical environments at Uxbenká, Belize. *J. Archeol. Sci.* 57, 1–13.
- Raney, R.K., 1998. Radar fundamentals: technical perspective. In: Henderson, F.M., Lewis, A.J. (Eds.), Manual of Remote Sensing. John Wiley Sons, Inc., New York, pp. 9–130.
- Proyecto arqueológico Yaxnöhcah, 2013. In: Reese-Taylor, K., Anaya Hernández, A. (Eds.), Informe de la Primera Temporada de investigaciones. University of Calgary, Calgary (56 pp.).
- Reese-Taylor, K., Anaya Hernández, A.A., Flores Esquivel, F.C.A., Monteleone, K., Uriarte, A., Carr, C., Geovannini Acuña, H., Fernandez-Díaz, J.C., Peuramaki-Brown, M., Dunning, N., 2016. Boots on the ground of Yaxnöhcah. *Adv. Archeol. Pract.* 4 (3), 314–338.
- Ruppert, K., Denison Jr., J.H., 1943. Archaeological Reconnaissance in Campeche, Quintana Roo, and Petén, Publication 543. Carnegie Institution of Washington, Washington DC.
- Saturno, W., Sever, T.L., Irwin, D., Howell, B., Garrison, T., 2007. Putting us on the map, remote sensing investigation of the ancient Maya landscape. In: Wiseman, J., El-Baz, F. (Eds.), *Remote Sensing in Archaeology. Interdisciplinary Contributions to Archaeology*. Springer, New York, pp. 137–160.
- Seefeld, N., 2013. Public provisions for dry seasons, the hydraulic system of Uxul and its relevance for the survivability of the settlement. *Contrib. New World Archeol.* 5, 57–84.
- Sever, T.L., 1998. Validating prehistoric and current phenomena upon the landscape of the Petén, Guatemala. In: Liverman, D., Moran, E.F., Rindfuss, R.R., Stern, P.C. (Eds.), *People and Pixels, Linking Remote Sensing and Social Science*. National Academy Press, Washington DC, pp. 145–163.
- Sever, T.L., Irwin, D.E., 2003. Landscape archaeology, remote-sensing investigation of the ancient Maya in the Petén rainforest of northern Guatemala. *Anc. Mesoam.* 14 (1), 113–122.
- Shaw, J.M., 2012. Roads to ruins, the role of sacerdotal in ancient Maya society. In: Alcock, S.E., Bodel, J., Talbert, R.J.A. (Eds.), *Highways, Byways, and Road Systems in the Pre-modern World*. Wiley-Blackwell, Oxford, pp. 128–146.
- Solberg, S., Weydahl, D.J., Næset, E., 2007. SAR forest canopy penetration depth as an indicator for forest health monitoring based on leaf area index LAI. In: Proc. 5th Int. Symp. Retrieval of Bio- and Geophysical Parameters from SAR Data for Land Applications, (5 pp.). (Bari Italy).
- Šprajc, I. (Ed.), 2008. Reconocimiento arqueológico en el sureste del estado de Campeche, México, 1996–2005. British Archeol. Rep., Oxford (290 pp.).
- Šprajc, I., Esquivel, A.F., Čaval, S., García López, M.I., Marsetić, A., 2010. Archaeological reconnaissance in southeastern Campeche, Mexico, summary of the 2007 field season. *Mexicon* 32 (6), 148–153.
- Stanton, T.W., Freidel, D.A., 2005. Placing the centre, centring the place, the influence of formative sacerdotal in the Classic site design at Yaxuná, Yucatán. *Camb. Archaeol. J.* 15 (2), 225–249.
- Stewart, C., Lasaponara, R., Schiavon, G., 2014. Multi-frequency polarimetric SAR analysis for archaeological prospection. *Int. J. Appl. Earth Obs.* 28, 211–219.
- Straulino, L., Sedov, S., Michelet, D., Balanzario, S., 2013. Weathering of carbonate material in ancient Maya constructions Rio Bec and Dzibanché, limestone and stucco deterioration patterns. *Quat. Int.* 315, 87–100.
- Suyuc-Ley, E., Hansen, R.D., 2013. El complejo piramidal La Danta, ejemplo del auge en El Mirador. In: Arnould, M.-C., Breton, A. (Eds.), *Millenary Maya Societies, Past Crises and Resilience*. Mesoweb, Paris, pp. 217–234.
- Tapete, D., Cigna, F., 2017. Trends and perspectives of space-borne SAR remote sensing for archaeological landscape and cultural heritage applications. *J. Archeol. Sci: Rep.* 14, 716–726.
- Turner II, B.L., Klepeis, P., Schneider, L.C., 2003. Three millennia in the southern Yucatán Peninsula, implications for occupancy use, and carrying capacity. In: Gómez-Pompa, A., Allen, M.F., Fedick, S.L., Jiménez-Orsonio, J.J. (Eds.), The Lowland Maya Area, Three Millennia at the Human-wildlife Interface. The Haworth Press Inc., New York, pp. 361–387.
- Wahl, D., Byrne, R., Anderson, L., 2014. An 8700 year paleoclimate reconstruction from the southern Maya lowlands. *Quat. Sci. Rev.* 103, 19–25.
- Weishampel, J.F., Hightower, J.N., Chase, A.F., Chase, D.Z., Patrick, R.A., 2011. Detection and morphologic analysis of potential below-canopy cave openings in the karst landscape around the Maya polity of Caracol using airborne LiDAR. *J. Cave and Karst Stud.* 733, 187–196.
- Weiss-Krejci, E., Sabbas, T., 2002. The potential role of small depressions as water storage features in the Central Maya Lowlands. *Lat. Am. Antiq.* 13 (3), 343–357.
- Witschey, W.R.T., Brown, C.T., 2017. The Electronic Atlas of Ancient Maya Sites. <http://MayaGIS.smv.org> [Electronic database graciously sent by the first author, January 19, 2017].